Articles relacionats amb el Capítol 1

Article A

Títol: Radical *para*-benzoic acid derivatives: Transmission of ferromagnetic interactions through hydrogen bonds at long distances

Autors: D. Maspoch, L. Catala, P. Gerbier, D. Ruiz-Molina, J. Vidal-Gancedo, K. Wurst, C. Rovira, J. Veciana.

Publicació: Chem. Eur. J. 2002, 8, 3635.

(Presentat a la Comissió de Doctorat).

Radical *para*-Benzoic Acid Derivatives: Transmission of Ferromagnetic Interactions through Hydrogen Bonds at Long Distances

Daniel Maspoch,[a] Laure Catala,[a] Philippe Gerbier,[b] Daniel Ruiz-Molina,[a] José Vidal-Gancedo,[a] Klaus Wurst,[c] Concepció Rovira,[a] and Jaume Veciana*[a]

Abstract: Investigation of the transmission of magnetic interactions through hydrogen bonds has been carried out for two different benzoic acid derivatives which bear either a *tert*-butyl nitroxide (NOA) or a poly(chloro)triphenylmethyl (PTMA) radical moiety. In the solid state, both radical acids formed dimer aggregates by the complementary association of two carboxylic groups though hydrogen bonding. This association ensured that atoms with most spin density are separated from one another by more than 15 Å. Thus, no competing through-space magnetic exchange interactions are expected in these dimers and, hence, they provide good models to investigate whether noncovalent hydrogen bonds play a role in the long-range transmission of magnetic interactions. The nature of the magnetic exchange interaction and their strengths within similar dimer aggregates in solution was assessed by electron spin resonance (ESR) spectroscopy. In the case of radical NOA, low-temperature ESR experiments showed a weak ferromagnetic interaction between the two radicals in the dimer aggregates (which have the same geometry as in the solid state). In contrast, the corresponding solution ESR study performed with radical PTMA did not lead to any conclusive results, as aggregates were formed by noncovalent interactions other than hydrogen bonds. However, the bulkiness of the poly(chloro)triphenylmethyl radical prevented interdimer contacts in the solid state between regions of high spin density. Hence, solid-state measurements of the α phase of PTMA radical provided evidence of the intradimer interaction to confirm the transmission of a weak ferromagnetic interaction through the carboxylic acid bridges, as found for the NOA radical. Moreover, crystallization of the PTMA radical in presence of ethanol to form the β phase of PTMA radical prevented the dimer formation; this resulted in the suppression of this interaction and provides further evidence of the magnetic exchange mechanism through noncovalent hydrogen bonds at long distances.

Keywords: dimerization · EPR spectroscopy · hydrogen bonds · radicals · through-bond interactions

Introduction

During the last decade, great interest has been focused on purely organic magnetic materials,[1] stimulated by the discovery of bulk ferromagnetism in α-nitronyl nitroxide derivatives at low temperatures.[2] Since ferromagnetism is a cooperative property, intermolecular magnetic interactions between the spin-bearing molecules must be controlled. Consequently, a well-designed purely organic magnetic material depends on two aspects: 1) the capacity to control the structural arrangement in the crystal and 2) the ability to predict the magnetic interactions that are associated with each arrangement. Crystal engineering through hydrogen bonds is a powerful method for achieving the first condition; that is, controlling the relative positioning of the neighboring molecules through the formation of well-defined supramolecular patterns in the solid state.[3] Nevertheless the role hydrogen bonds play in the transmission of magnetic interactions is still not completely understood. Several groups have taken advantage of this noncovalent approach in designing organic ferromagnets.[4–14] Most reported examples are based on α-nitronyl nitroxide, α-imino nitroxide, or *tert*-butyl nitroxide derivatives because of their high stability and the ability of their nitroxide (NO) groups to act as acceptors of hydrogen bonds. A strategy that has been used with these radicals combines the nitroxide radical with a diamagnetic compound that bears an appropriate hydrogen-bond donor group for the formation of hydrogen-bonded networks.[4, 5] Nevertheless,

[a] Prof. J. Veciana, D. Maspoch, Dr. L. Catala, Dr. D. Ruiz-Molina, Dr. J. Vidal-Gancedo, Dr. C. Rovira
Institut de Ciència de Materials de Barcelona (CSIC)
Campus Universitari de Bellaterra, 08193 Cerdanyola (Spain)
Fax: (+34) 393-580-5729
E-mail: vecianaj@icmab.es

[b] Dr. P. Gerbier
Laboratoire de Chimie Moléculaire et Organisation du Solide
UMR-5637, Université Montpellier 2, Place E. Bataillon
34095 Montpellier (France)

[c] Dr. K. Wurst
Institut für Allgemeine Anorganische und Theoretische Chemie
Universität Innsbrück, 6020, Innrain 52a (Austria)

  0947-6539/02/0816-3635 $ 20.00+.50/0

this strategy leads to a dilution of the magnetically active units in the solid and, therefore, to an increase of their separation, which in turn decreases the strength of intermolecular magnetic interactions. To avoid such drawbacks, the hydrogen-bond donor groups can be directly introduced on the molecule that bears the radical, so that self-assembled patterns can be formed directly between the paramagnetic molecules. An alternative approach is to use magnetically active transition metal ions as hydrogen-bond acceptor species and those radicals as ligands. These approaches have been successfully applied to nitroxide radicals with various substituents such as phenol,[6] boronic acid,[7] imidazole,[8] benzimidazole,[8, 9] triazole,[10] uracil,[11] pyrazole,[12] phenyl acetylene,[13] or benzoic acid.[14, 16–19] Besides their structural control, hydrogen bonds have also been shown to favor magnetic exchange interactions between bound radical molecules. Thus, in the solid state, a few examples have illustrated the propagation of magnetic exchange through strong (OH···O) and weak (CH_3···O) hydrogen bonds.[4, 6] Furthermore, polarized neutron diffraction experiments, which were performed on an α-nitronyl nitroxide acetylenic derivative, have provided an example in which spin density is transferred through the covalent framework from the NO group to a H atom on a ethynyl group, which is involved in a intermolecular hydrogen bond.[13] With the design of radical molecules that bear hydrogen-bond donor and acceptor groups, the structural dimensionality of the material may be controlled to some extent and, hence, also the propagation of the magnetic interactions through the supramolecular structure. However, the difficulty lies in the determination of the strength and nature of the magnetic interaction through this supramolecular pathway, since many other intermolecular interactions compete in the solid state. An interesting way to avoid this complexity is to obtain oligomers (dimers, trimers, etc.) with well-defined geometries in solution, since such supramolecular entities are isolated from each other and, therefore, other types of intermolecular interactions would not be present.[6e, 11, 12, 17] The main problem in these supramolecular aggregates is that NO groups are often involved in hydrogen bonds and this gives rise to cyclic dimers or trimers with their regions of radical spin density quite close to one another. To find suitable radicals that form hydrogen-bonded supramolecular aggregates in solution and in which the radicals centers are far enough away for a direct through-space magnetic interaction, we designed the two open-shell *para*-benzoic acid derivatives that bear either a *tert*-butyl nitroxide group in the case of the radical NOA (**1**) or a polychlorinated triphenylmethyl radicalin the case the radical PTMA (**2**), as open-shell moieties. The general trend of carboxylic acids to form dimers,

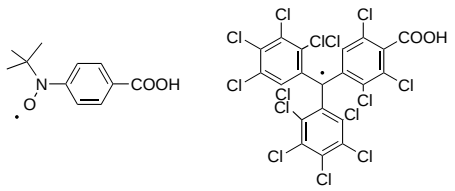

NOA (**1**) PTMA (**2**)

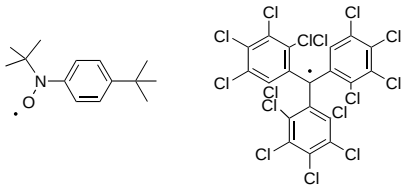

NO*t*Bu PTMCl

both in solution and in solid state,[15] suggested that both radicals would be ideal systems to show whether the propagation of the magnetic exchange is efficient at a long distance. Indeed, the ring pattern that they may form through the two complementary carboxylic groups could prevent the atoms with most of the radical spin density from approaching each other. These compounds provide a good model for the study of the magnetic exchange interaction through non-covalent hydrogen bonds without perturbations from direct

Abstract in Catalan: *La investigació de les transmissions d'interacció magnètica s'ha portat a terme utilitzant dos derivats diferents d'àcid benzoic, més concretament les espècies radicalàries nitròxid tert-butílic (NOA) i policlorotrifenilmetil (PTMA). En ambdós radicals, s'han observat agregats dimèrics en estat sòlid, formats per l'associació complementària dels grups carboxílics mitjançant enllaços d'hidrogen. Aquesta associació assegura que els àtoms amb major densitat d'espí estiguin allunyats amb distàncies més llargues que 15 Å els uns respecte als altres. Aquest fet origina que en aquests dímers no s'esperin altres interaccions d'intercanvi magnètic a través de l'espai, essent bons models per observar quin paper juguen els enllaços d'hidrogen en la transmissió d'interaccions magnètiques a distàncies llargues. Un altre camí per determinar la naturalesa i força de les interaccions d'intercanvi magnètic era estudiar la mateixa classe d'agregats en solució mitjançant l'espectroscòpia de RPE. En el cas del radical NOA, experiments de RPE a temperatura baixa van evidenciar la presència d'interaccions ferromagnètiques dèbils entre els dos radicals dels agregats dimèrics, els quals tenen la mateixa geometria que en estat sòlid. A diferència, estudis similars de RPE amb el radical PTMA no van portar a cap conclusió, degut a que en solució es formaven altres agregats no covalents a més dels de naturalesa d'enllaços d'hidrogen. No obstant, degut a la grandària dels radicals policlorotrifenilmetílics, es van negligir els contactes entre regions on la densitat d'espí és més elevada entre diferents dímers en estat sòlid. Així, les mesures del radical PTMA (fase alfa) en estat sòlid van aportar evidències clares sobre la interacció a dins d'un dímer, la qual va confirmar la transmissió d'interaccions ferromagnètiques dèbils a través de ponts d'àcid carboxílic, a l'igual que en el radical NOA. A més, la cristallització del radical PTMA en presència d'EtOH, que dóna lloc a la fase β del radical PTMA, preveu la formació dels dímers, suprimint així aquesta interacció i donant més evidències del mecanisme d'intercanvi magnètic mitjançant enllaços d'hidrogen no covalents a distàncies llargues.*

  0947-6539/02/0816-3636 $ 20.00+.50/0 *Chem. Eur. J.* **2002**, *8*, No. 16

through-space interactions. We describe herein the synthesis and extensive magnetic studies, both in solution and in the solid state, of these two radicals and show that magnetic exchange interactions are transmitted efficiently through the hydrogen bonds that form between the two COOH groups.

Results and Discussion

Synthesis: Radical NOA was synthesized by a three-step procedure from 1-[*N*-*tert*-butyl-*N*-(*tert*-butyldimethylsiloxy)amino]-4-bromobenzene (**3**),[20] as shown in Scheme 1. The carboxylic acid function was introduced by the reaction of the lithiated derivative **4** with CO_2 and then the removal of the protecting group with fluoride ions. The oxidation of the hydroxylamine **5** by PbO_2 afforded the NOA radical (**1**) as a crystalline red-orange solid. Red-orange needle-shaped crystals were obtained by crystallization from dichloromethane. PTMA (**2**) was synthesized according to the procedure described in the literature.[20] The crystallization of this radical was performed by diffusion of hexane into a dichloromethane solution of the radical to form the α phase as red thin plates. This crystalline phase is a clathrate compound that contains two molecules of dichloromethane in the unit cell. The β phase was formed as red needles by slow evaporation of a solution of the radical from EtOH. This phase is also a clathrate compound that contains three molecules of ethanol to two radicals.

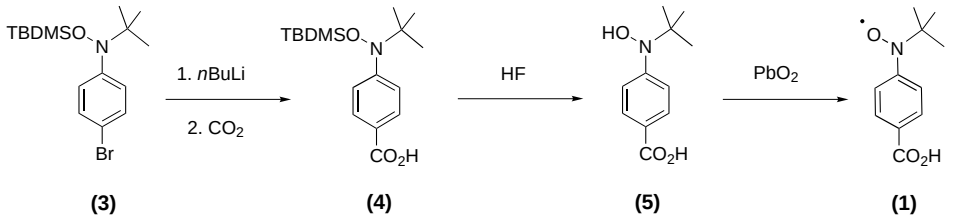

(3) **(4)** **(5)** **(1)**

Scheme 1. Synthesis of the NOA radical.

Crystal structures: Radical NOA crystallizes in the $P2_1/n$ monoclinic space group and the cell parameters are reported in Table 1. The asymmetric unit (Figure 1a) has a conformation in which the torsion angle between the benzene ring and the carboxylic group is 3.8°. The normal to the plane defined by the $C_{ar}NO$ atoms makes an angle of 18.3° with the normal to the phenyl ring. This value is well within the range of crystallographic values for related molecules. Thus, this radical adopts a nearly planar conformation, which seems to be favored by the weak intramolecular hydrogen bonds between the aromatic H atoms and the O atoms of carboxylic acid (O2···HC4, 2.51 Å; C4-H-O, 98°) and the NO groups (O3···HC3, 2.37 Å; C3-H-O, 99°). In most of dimers previously reported for other carboxylic acids, the C=O and C–OH atoms are often disordered,[22] and this gives rise to apparent equivalent C–O bond lengths. However, in this case, two nonequivalent C–O bonds are found (C8–O2, 1.237(2) Å and C8–O3, 1.302(2) Å). These bond lengths correspond to the C=O and C–OH bonds, respectively. Again, this feature seems to be due to the weak intramolecular hydrogen bonds which lock the oxygen of the C=O group in the O2 rather than the O3 position.

Table 1. Crystallographic parameters of NOA and PTMA radicals.

	NOA	PTMA (α phase)	PTMA (β phase)
formula	$C_{11}H_{14}N\,O_3$	$C_{20.5}H_2Cl_{15}O_2$	$C_{23}H_{10}Cl_{14}O_{3.50}$
M_r	208.23	811.97	838.61
lattice type	monoclinic	Triclinic	Triclinic
space group	$P2_1/n$	$P\bar{1}$	$P\bar{1}$
a [Å]	6.8949(5)	8.8400(3)	8.816(2)
b [Å]	8.7147(3)	12.8188(5)	13.840(4)
c [Å]	18.377(1)	14.3719(6)	14.379(5)
α [°]	90	96.461(2)	66.645(8)
β [°]	92.427(2)	97.378(2)	79.87(2)
γ [°]	90	98.607(2)	88.20(2)
V [Å^3]	1103.23(11)	1582.44(11)	1584.2(8)
Z	4	2	2
ρ_{calcd} [g cm^{-3}]	1.254	1.704	1.758
T [K]	218	223	223
reflections measured	1626	4665	2138
reflections observed [$I > 2\sigma(I)$]	1355	4058	1474
$R1$ [$I > 2\sigma(I)$]	0.0374	0.0494	0.0743
$R1$ (all data)	0.0466	0.0605	0.1159
$wR2$ (all data)	0.1023	0.1852	0.1846

Complementary hydrogen bonding between the two carboxylic groups of neighboring radicals (O2···HO3, 1.64 Å; O2-H-O3, 176°) generated, as the *primary crystalline pattern*, the hydrogen-bonded dimers shown in Figure 2a. The eight-membered ring formed by the hydrogen-bonded carboxylic acid fragments lies in the plane of the benzene rings as the torsion angle between the carboxylic group and the benzene ring is small. The molecules that are related by the inversion center of the unit cell are $\pi-\pi$ stacked with a distance of 3.66 Å between the aromatic rings. Furthermore, the molecules are also related along the *a* axis by two sets of weak hydrogen bonds that involve an aromatic H atom of one molecule and the NO (O1···HC3, 2.65 Å; C3-H-O, 134°) and carboxylic groups (O3···HC6, 2.57 Å; C6-H-O, 135°) of neighboring molecules. These contacts connect the dimers together into distinct layers, A and A′, within the *ab* plane; this constitutes the *secondary crystalline pattern* (Figure 2b). Layers A and A′ are further connected along the *c* direction by two weak hydrogen bonds between the *tert*-butyl and carboxylic groups of one molecule (O2···HC12, 2.60 Å; C12-H-O2, 170°) and the NO group (O1···HC13, 2.81 Å; C13-H-O1, 160°) of the neighboring molecule. Finally, the long separation of the two NO groups within the dimers is notable (15.15 Å), while the shortest contact between NO groups is 6.08 Å between the N atoms of the $\pi-\pi$ stacked molecules.

As already mentioned, radical PTMA crystallizes in two polymorphs, α and β, which depend on the crystallization conditions. The α phase crystallizes in the $P\bar{1}$ triclinic space group and the cell parameters are reported in Table 1. A molecule of dichloromethane is included in the cell with the

  0947-6539/02/0816-3637 $ 20.00+.50/0

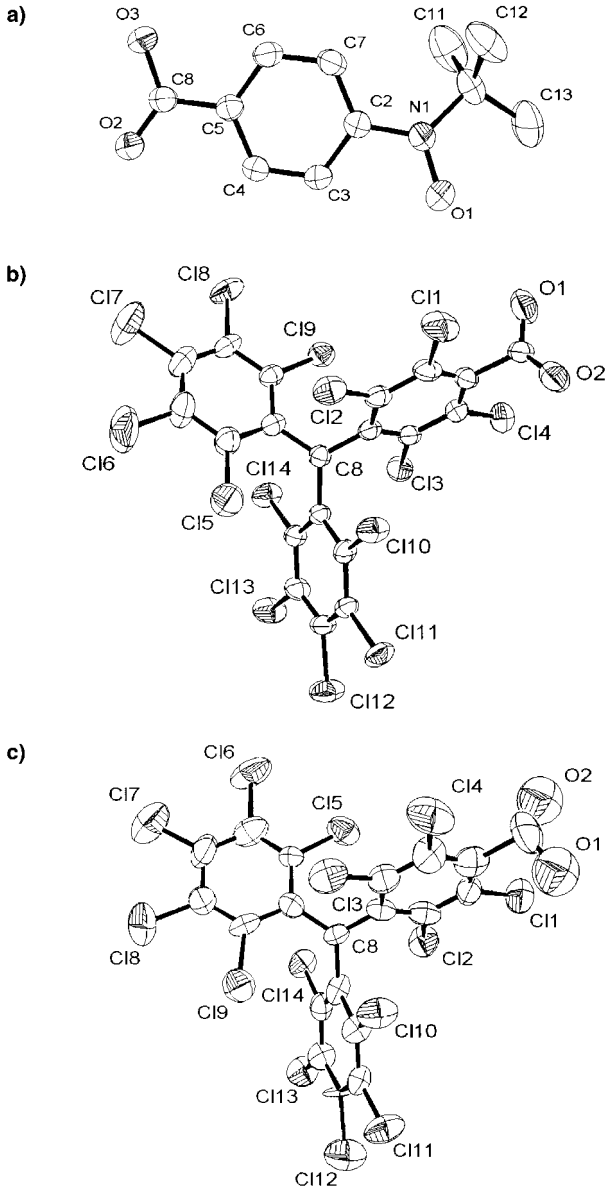

Figure 1. ORTEP representations of molecules found in a) radical NOA, b) the α phase of radical PTMA, and c) the β phase of radical PTMA in which the two carboxylic groups are present with a probability factor of 0.5.

PTMA radical in a 2:1 ratio. This clathrate compound is stabilized by a short Cl$\cdots$Cl contact (Cl15$\cdots$Cl9, 3.44 Å). In contrast to the NOA radical, the carboxylic group is disordered as two equivalent C–O bond lengths (C–O1, 1.218(6) Å and C–O2, 1.230(6) Å) are found. The absence of any stabilization of the C=O bond in one position by the weak hydrogen bonds accounts for this difference. The torsion angles between the mean planes of the three polychlorinated aromatic rings and that of the three bridgehead and one methyl C atoms (the reference plane) are 46, 51, and 55°. These angles generate the propeller-shape conformation which is usually found in this family of radicals (Figure 3a).[23] Due to the steric hindrance from the chlorine atoms *ortho* to the carboxylic group, the carboxylate is twisted by 88° with respect to the phenyl plane to which it is bonded. The primary crystalline pattern of the α phase is also a hydrogen-bonded

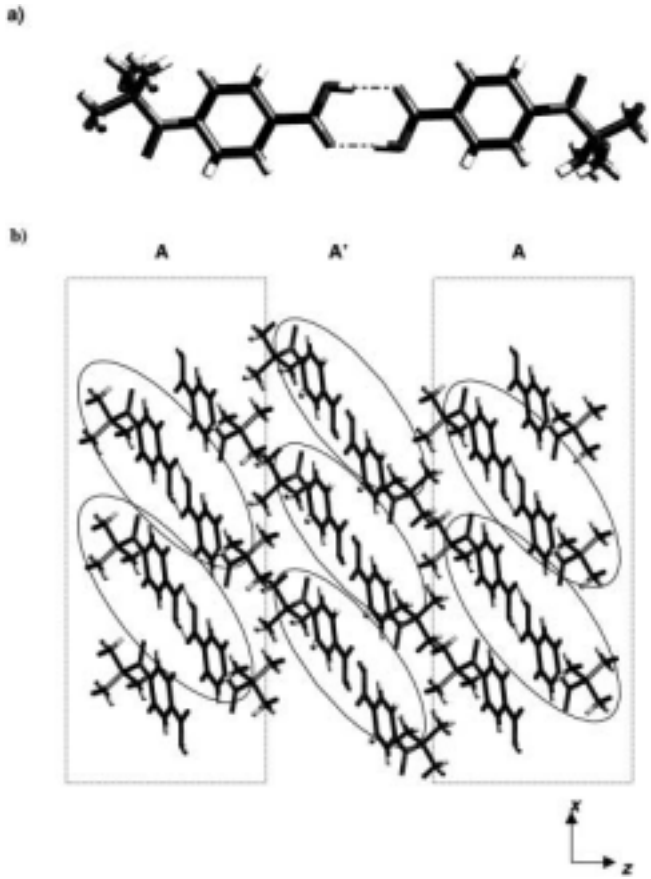

Figure 2. a) View of the hydrogen-bonded dimer formed by radical NOA in the solid state b) View along the *b* axis of the primary and the secondary crystalline patterns.

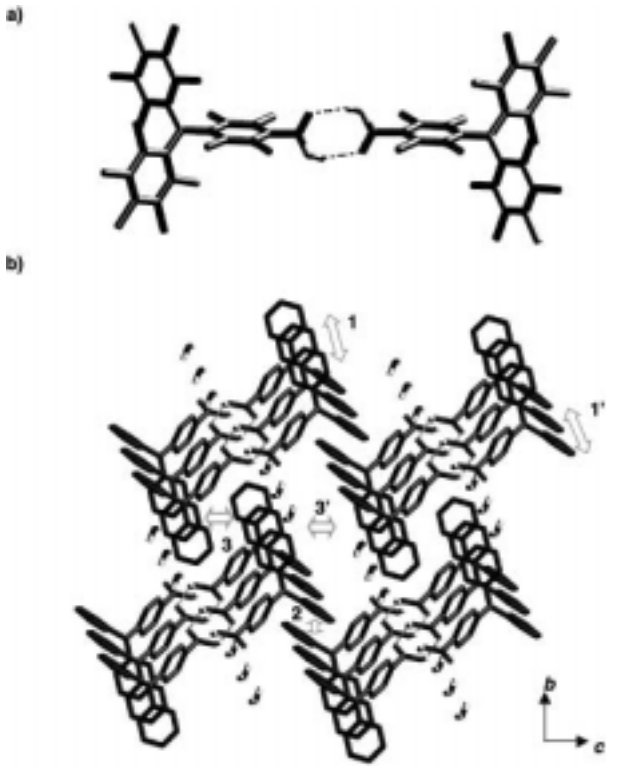

Figure 3. a) View of hydrogen-bonded dimer in the α phase of radical PTMA. b) Representation along the *a* axis of the shortest contacts in the molecular packing of α phase of PTMA.

0947-6539/02/0816-3638 $ 20.00+.50/0 *Chem. Eur. J.* **2002**, *8*, No. 16

dimer formed through the two carboxylic groups (O1 ··· H-O2, 1.955 Å; O1-H-O2, 144°), as shown in Figure 3a. These dimers are connected to each other through short Cl ··· Cl contacts, as shown in Figure 3b. In the *a* direction there are two such contacts (1 and 1′: Cl(9) ··· Cl(1), 3.35 Å; Cl(10) ··· Cl(13), 3.40 Å, respectively), whereas only one contact is present in the *b* direction (2: Cl(4) ··· Cl(7), 3.46 Å) and two further contacts in the *c* direction are observed (3 and 3′: Cl(2) ··· Cl(8), 3.33 Å; Cl(5) ··· Cl(5), 3.22 Å, respectively). The shortest distance between the methyl C atoms of neighboring radicals is found within the dimers at a length of 15.36 Å.

In the β phase of radical PTMA, molecules crystallize in the $P\bar{1}$ triclinic space group and cell parameters are given in Table 1. The PTMA molecules also adopt a propeller-shape conformation with torsion angles of 45, 51, and 54° between the mean planes of the aromatic rings and the reference plane. The carboxylic acid group in this phase has an angle of around 89° with respect to the aromatic plane and is disordered with a 0.5 occupancy factor for the C12 and C2 atoms. This is shown on the ORTEP view (Figure 1c). There are ethanol molecules in the unit cell in a 1.5:1 ratio with PTMA and these form three different hydrogen bonds with the carboxylic acid (hydrogen bond 1: O2 ··· H-O5, 2.39 Å; O2-H-O5, 109°; hydrogen bond 2: O1 ··· H-O6, 2.52 Å; O1-H-O6, 124°; and hydrogen bond 3: O6 ··· H-O1, 2.37 Å; O6-H-O1, 139°). There is also an additional hydrogen bond between two of the EtOH molecules (hydrogen bond **4**: O5 ··· H-O6, 2.12 Å; O5-H-O6 142°). By bonding to the carboxylic group, EtOH prevents the formation of the dimer aggregates of PTMA that are found in the α phase. Thus, the primary crystalline pattern of the β phase consists of two molecules of PTMA with three molecules of EtOH in between them, as shown in Figure 4a. These patterns are related to each other by short Cl ··· Cl contacts. In the *a* direction, two of such contacts are present (1 and 1′: Cl5 ··· Cl4, 3.43 Å; Cl10 ··· Cl13, 3.42 Å), whereas only one such contacts is present in the *b* direction (2: Cl2 ··· Cl11, 3.46 Å) and two others in the *c* direction (3 and 3′: Cl14 ··· Cl8, 3.39 Å; Cl5 · · · Cl5, 3.22 Å).

Magnetic characterization—ESR solution studies: To get an overview of the unpaired electron delocalization on NOA and PTMA radicals, as well as to study the supramolecular aggregation they undergo in solution, X-band ESR spectra of dilute fluid and rigid (frozen) solutions were recorded under different experimental conditions.

Radical NOA: The room-temperature spectrum of NOA at a concentration of 1.0×10^{-4} M in dichloromethane consists of three overlapped groups of lines with 1:1:1 intensities, due to the hyperfine coupling of the unpaired electron with the nuclear spin of the N atom (Figure 5). The further splitting of each of these groups of lines arises from the additional coupling of the unpaired spin with the four H nuclei from the aromatic ring (two equivalent *ortho* H and two equivalent *meta* H nuclei). The coupling with the nine equivalent H atoms of the *t*Bu group is unresolved under these conditions. The whole spectrum can be simulated with the isotropic hyperfine coupling constants shown in Table 2; the simulated

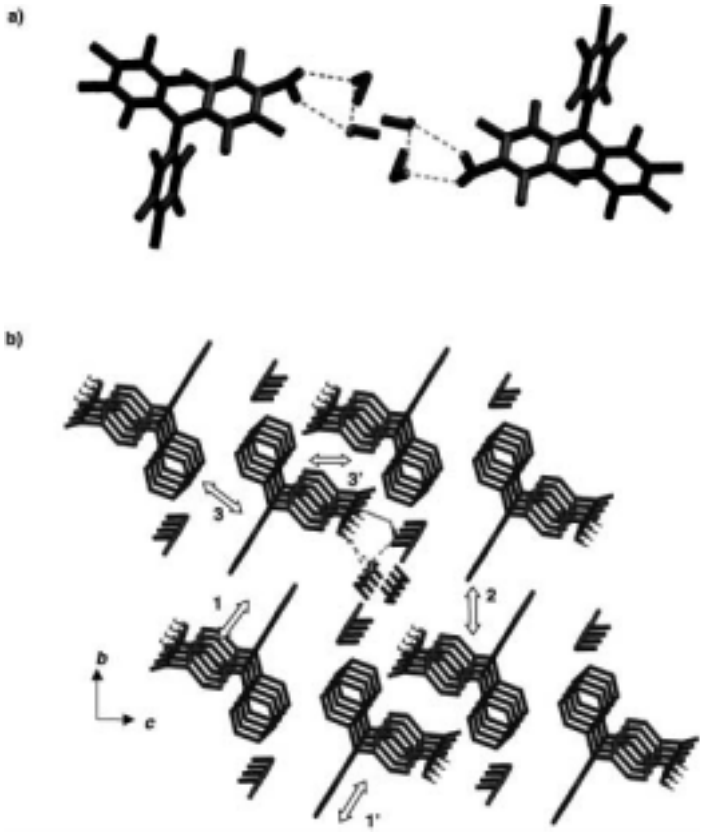

Figure 4. a) View of hydrogen-bonded dimer in the β phase of radical PTMA. The central EtOH molecules are disordered in the two depicted positions. b) Representation along the *a* axis of the shortest contacts in the molecular packing of β phase of PTMA.

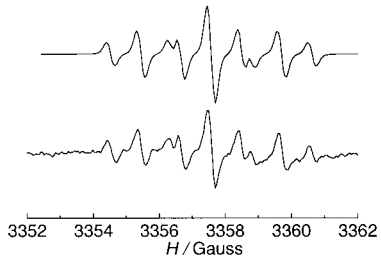

Figure 5. ESR spectra of NOA in a dilute dichloromethane solution at room temperature. Bottom: experimental spectrum: frequency: 9.392353 GHz; power: 5.090 W; modulation amplitude 0.2 G. The intensities of the two starred lines change with temperature and concentration (see text). Top: simulation of the spectrum, parameters in Table 2.

Table 2. Hyperfine coupling constants from simulation of ESR spectra of dilute solutions of radicals NOA and PTMA.

	Concentration [M]	a_N [Gauss]	$a_{H\text{-}ortho}$ [Gauss]	$a_{H\text{-}meta}$ [Gauss]	$a_{C\text{-}methyl}$ [Gauss]	$a_{C\text{-}ortho}$ [Gauss]	$a_{C\text{-}bridgehead}$ [Gauss]
NOA[a]	1.0×10^{-4}	11.57	2.13	0.92	–	–	–
NOA[b,d]	5.3×10^{-3}	11.00	2.30	0.92	–	–	–
		5.50	1.15	0.46			
NO*t*Bu[b]	5.3×10^{-3}	12.50	2.14	0.92	–	–	–
PTMA[c]	1.0×10^{-4}	–	–	–	30.0	13.1	10.7
PTMA[b]	1.0×10^{-4}	–	–	–	29.5	12.9	10.6
PTMCl[b]	5.3×10^{-3}	–	–	–	29.5	12.9	10.5

[a] Performed in CH_2Cl_2 at room temperature. [b] Performed in CH_2Cl_2/toluene (1:1) at 200 K. [c] Performed in CH_2Cl_2/toluene (1:1) at room temperature. [d] Biradical:radical molar ratio was of 3.1:1.0.

  0947-6539/02/0816-3639 $ 20.00+.50/0

spectrum is shown on the top of Figure 5. An interesting observation is the slight decrease in the hyperfine coupling of the N atom in radical NOA with respect to that of the *para tert*-butyl benzene derivative, NO*t*Bu, which was obtained under similar experimental conditions. This indicates that the unpaired electron is somewhat more delocalized on the aromatic ring of the radical NOA than in NO*t*Bu, due to the conjugation effect of the carboxylic group.[24, 25] The spectrum of radical NOA varies significantly as the radical concentration and the temperature are changed; additional lines appear at intermediate positions (starred in Figure 6) and increase in

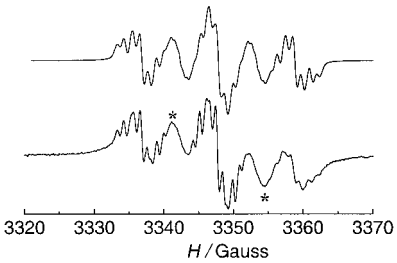

Figure 6. ESR spectrum of dilute solution of NOA in toluene/dichloromethane at 180 K. Concentration: 5.3×10^{-3} M; frequency: 9.395658 GHz; power: 1.016×10^{-1} mW; modulation amplitude: 0.403 G.

intensity as the temperature is lowered or the concentration is increased. These changes are reversible and indicate the formation of other paramagnetic species due to an aggregation phenomenon; that is, the establishment of equilibrium between radical molecules and supramolecular aggregates that can be shifted towards the aggregates when temperature is lowered or the concentration increased. The nature of these aggregates was investigated with a 5.3×10^{-3} M solution of NOA in dichloromethane/toluene (1:1 v/v). As shown in Figure 6, the experimental spectrum at 180 K is reproduced by the addition of the simulated spectrum of the monoradical with that of a dimer in a molar ratio of 1:3. For the simulation of the dimer, half the values of hyperfine coupling constants, a_N and a_H, of the monoradical and its g factor were used. Besides the dimeric nature of the aggregates, this result suggested that the two unpaired electrons of the dimer interact magnetically within the so-called "strong exchange limit" so that the exchange coupling constant J is much greater than a_N.[25b, 26] The dimeric nature of aggregates was further confirmed by the spectrum of the frozen solution, since both the fine structure and the half-field signal characteristic of a triplet species ($S = 1$) were observed (vide infra).

In principle, dimers of NOA may have several different geometries that depend on the nature and strength of the different interactions ($\pi - \pi$, strong and weak hydrogen bonds, etc.) which join the two radical moieties. Regardless of the nature and strength of these interactions, aggregates must be favored by increased radical concentration, so that above a certain concentration level, several kinds of aggregates may coexist. To exclude all aggregates formed by weak interactions and to limit the study only to those linked by strong hydrogen bonds, that is, aggregates formed by strong nitroxide/acid or acid/acid hydrogen bonds (see Scheme 2), it

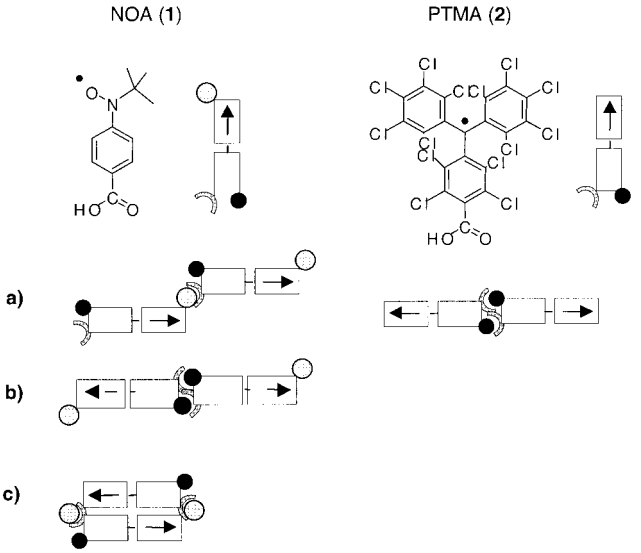

Scheme 2. Schematic representation of potential dimer aggregates which may form in solutions of NOA and PTMA radicals.

was important to determine the critical concentration below which only strong hydrogen bonds occur. We used the radical NO*t*Bu,[24] as a reference molecule, as it cannot be involved in any strong hydrogen-bond interactions and undergoes aggregation through other weak interactions. The spectrum of a 5.3×10^{-2} M solution of radical NO*t*Bu in dichloromethane/toluene (1:1 v/v) did not show any intermediate lines at room temperature; this suggested the unique presence of monomeric radicals. However, the frozen solution exhibited a half-field signal, which revealed that other kinds of aggregates form in solution. The solution was diluted to a value of 5.3×10^{-3} M, which ensured the absence of the half-field signal even at low temperatures and showed that aggregation phenomenon did not take place. Consequently, this concentration was adopted as the higher concentration limit for the study of the hydrogen-bonded dimers of NOA. Figure 7 shows the ESR spectrum of a frozen solution of NOA at 106 K at a concentration of 5.3×10^{-3} M in dichloromethane/toluene (1:1 v/v), in which the fine structure and half-field signal, which correspond to the $\Delta m_S = \pm 1$ and $\Delta m_S = \pm 2$ transitions of a triplet species ($S = 1$), respectively, are clearly observed. The presence of hydrogen bonds in such triplet species was confirmed by adding EtOH to the solution, which suppressed the half-field signal and gave a completely different $\Delta m_S = \pm 1$ signal, which was simulated with the parameters from Table 3, and which corresponds to a randomly oriented ensemble of monomeric radicals.

As shown in Scheme 2, dimer aggregates which are linked by strong hydrogen bonds may have either a linear or a cyclic geometry. In the first case the two radical moieties could be joined either by a single nitroxide/acid hydrogen bond (aggregate **a**) or by two complementary acid/acid hydrogen bonds (aggregate **b**), whereas in the cyclic case the radicals would be joined by two complementary nitroxide/acid hydrogen bonds (aggregate **c**). At first glance, aggregate **a** seems improbable, since the two other alternatives are energetically more favored by the formation of two hydrogen bonds instead

0947-6539/02/0816-3640 $ 20.00+.50/0 *Chem. Eur. J.* **2002**, *8*, No. 16

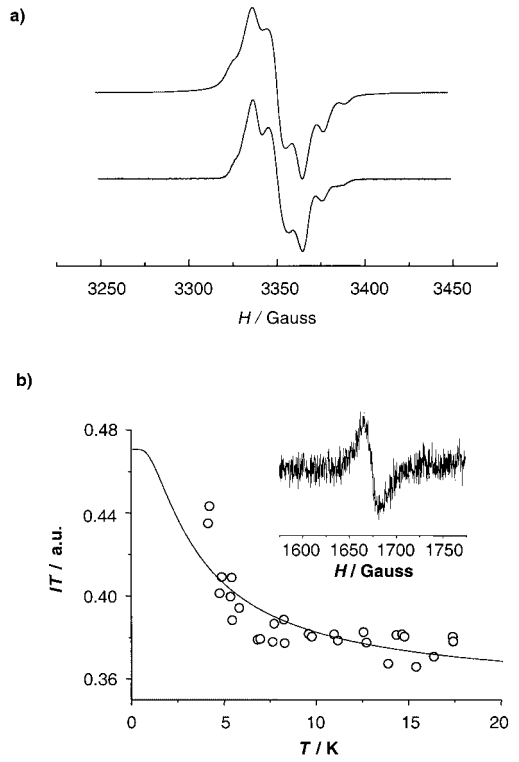

Figure 7. a) Experimental $\Delta m_S = \pm 1$ signal of NOA at 109 K (bottom). Concentration: 5.3 ± 10^{-3} M; frequency: 9.405598 GHz; power: 1.016×10^{-1} mW; modulation amplitude: 0.403 G. Simulated signal (top), parameters in Table 3. b) Temperature dependence of the peak–peak intensity, I_{pp}, plotted as $I_{pp}T$ product versus T, which corresponds to the $\Delta m_S = \pm 2$ transition. The solid line is the best fit of the experimental data to the Bleaney–Bowers equation. Inset: Observed $\Delta m_S = \pm 2$ signal at 109 K.

Table 3. ESR parameters used for the simulation of $\Delta m_S = \pm 1$ signals of monoradical and diradical aggregates of NOA in solution at 106 K.

Species	Components of $\boldsymbol{g}$ tensor	Components of $\boldsymbol{A}$ tensor[c]	D' [Gauss]	E' [Gauss]	B_{pp} [Gauss]
monoradical[a]	$g_{xx} = 2.0070$	$A_{xx} = 4.2$	–	–	$B_x = 8$
	$g_{yy} = 2.0070$	$A_{yy} = 4.2$			$B_y = 8$
	$g_{zz} = 2.0022$	$A_{zz} = 26.3$			$B_z = 9$
diradical[b]	$g_{xx} = 2.0070$	$A_{xx} = 2.1$	6.5 ± 1	0.0	$B_x = 15$
	$g_{yy} = 2.0070$	$A_{yy} = 2.1$			$B_y = 15$
	$g_{zz} = 2.0022$	$A_{zz} = 13.0$			$B_z = 3.5$

[a] In a 1:1 dichloromethane/toluene mixture with 3% of EtOH. [b] In a 1:1 dichloromethane/toluene mixture. [c] Components of the hyperfine coupling tensor with the N nuclei, assuming that $\boldsymbol{A}$ and $\boldsymbol{g}$ tensors are colinear.

of one. The most probable aggregates, diradicals **b** and **c**, can be distinguished by their zero-field-splitting (ZFS) parameters D' and E'. D' is related to the effective interspin distance, r, which can be calculated from the distance between the spin-bearing sites in the point dipole approximation by $D' = 27887/r^3$, in which D' is given in Gauss and r in Å. In contrast, the E' parameter simply relates to the symmetry of the diradical. Assuming that the spin density of aggregates **b** and **c** is mostly localized in two points around the two NO groups, r will be approximately twice the length for linear aggregate **b** than for cyclic **c**; therefore, the value of D' will be very different in both types of aggregates.

Hence, from the D' value, obtained from the simulation of experimental spectrum (see Table 3), a value of $r = 16.2$ Å was determined for the dimer aggregates present in solution. This value is close to the separation of the N and O atoms ($r_{N-N} = 15.1$ Å and $r_{O-O} = 16.4$ Å) determined in the solid state for the **b**-type dimers. Alternatively, if type **c** aggregates were formed, the separation would be less than 8 Å; hence this hypothesis must be discarded. Another estimate of r of the of NOA radical aggregates can be obtained from the relative intensity of the signal of the half-field transition, $I(\Delta m_s = \pm 2)$, to the signal, $I(\Delta m_s = \pm 1)$, of the allowed transition, since such a relative intensity is directly proportional to r^{-6}.[27] The proportionality constant depends on the nature of radical center, but in the case of the nitroxyl radical, which has an r value of 9–12 Å, it has been determined by Dubinskii et al.[28] to be 38 Å^6. Hence, the relative intensity, $I(\Delta m_s = \pm 2)/I(\Delta m_s = \pm 1)$, is obtained by the integration of the signal after correction for the content of free monomer radical, and a distance of 14.9 Å was determined. This result confirmed that radical NOA forms aggregates of type **b** in solution.

Another important aim of this study was to determine the nature and the strength of the magnetic exchange interactions that propagate within the aggregates through the hydrogen bonds at a long distance. To do so, the temperature dependence of the peak-to-peak intensity (I_{pp}) of the half-field signal was determined in the 4–100 K temperature range. The $I_{pp}T$ product plotted against temperature (Figure 7b) revealed the presence of ferromagnetic interactions within the dimers and demonstrated that the triplet is the ground state. Finally, the strength of the interactions within the dimer was determined by fitting the temperature dependence of I_{pp} to the Bleaney–Bowers equation,[29] which gave a value for the exchange coupling constant $J/k_B = 2.0 \pm 0.5$ K (using the Hamiltonian $\mathscr{H} = -2J(S_A \cdot S_B)$). This result demonstrates the efficiency of the coupling through a hydrogen bond even at long distances by using strongly delocalized radicals. The mechanism of ferromagnetic interaction is not clear, but it could be explained by the spin polarization mechanism (Scheme 3) if a regular alternation of the spin density on all the nuclei of the dimer with a significant value on the two H nuclei of hydrogen-bonded CO_2H groups is assumed.

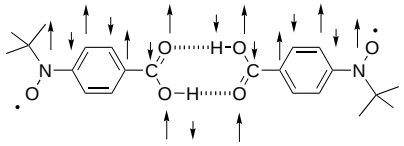

Scheme 3. Schematic representation of alternating spin densities in the hydrogen-bonded dimers of radical NOA.

Radical PTMA: The room-temperature ESR spectrum of radical PTMA in dichloromethane/hexane (1:1 v/v) shows one central main line surrounded by few weak satellite lines (Figure 8). These satellite lines originate from the hyperfine coupling of the unpaired electron with magnetically active ^{13}C nuclei in natural abundance at the α, bridgehead, and *ortho* positions. The experimental spectrum can be simulated by using the isotropic hyperfine coupling constants reported in

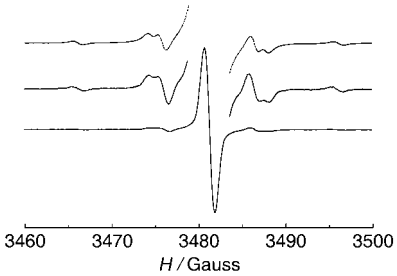

Figure 8. Experimental ESR spectrum (bottom) of a dilute solution of PTMA in toluene/dichloromethane (1:1 v/v) at room temperature. Concentration: 1×10^{-4} M; frequency: 9.756698 GHz; power: 5.090×10^{-1} mW; modulation amplitude: 1.0 G. Experimental spectrum (middle) in which the central line has been enlarged in order to observe the satellite lines. Simulated spectrum (top), parameters in Table 2.

Table 2; the simulated spectrum is shown in Figure 8. No significant differences were seen between the hyperfine coupling constants of this radical and that of radical PTMCl,[30] under similar experimental conditions; this indicates that the replacement of a Cl atom by a COOH group does not produce any noticeable change of the spin-density distribution.

To study the hydrogen-bonding aggregation phenomenon of radical PTMA in solution, the effect of concentration and temperature on the ESR spectra were studied for this radical and for reference radical PTMCl,[31]. ESR spectra, which were obtained at 111 K for solutions of the PTMCl radical of concentration 5.3×10^{-3} and 2.7×10^{-3} M in a dichloromethane/toluene (1:1 v/v), contained a significant half-field signal indicative of aggregate formation by interactions other than hydrogen-bonding. This tendency is specific to this family of compounds,[29] and may be explained by $Cl \cdots Cl$ and $\pi \cdots \pi$ interactions between aromatic rings of neighboring radicals, as these interactions are always present in their crystal structures. When the concentration of PTMCl was further lowered to 1.0×10^{-3} M, no half-field signals were detected; this suggests that at this critical concentration no aggregates were formed. This limiting concentration was thus used to study the aggregation of radical PTMA. However, at this concentration the spectrum of PTMA did not exhibit a half-field signal either, indicating that this concentration is also too low to induce hydrogen-bonded dimers. In contrast with NOA, no critical concentration was found in which only hydrogen-bonded dimers of PTMA were formed without the presence of other parasite aggregates.

To see if other information could be extracted about the size and nature of the aggregates, the ESR spectra of a concentrated solution of PTMA at 5.3×10^{-2} M was examined. The ESR spectrum in isotropic conditions (fluid solution) only showed the typical features of the monomer, although it is possible that the presence of exchange narrowed lines from dimers are hidden under the broad lines of monomer. In frozen solution (Figure 9), a signal from $\Delta m_S = \pm 1$ was observed as one weakly resolved line and there were no significant changes in comparison to the spectrum from dilute 1.0×10^{-3} M solution. Interestingly, a $\Delta m_S = \pm 2$ half-field signal was observed in the spectrum of the concentrated solution as a broad unresolved line. As a consequence, we may

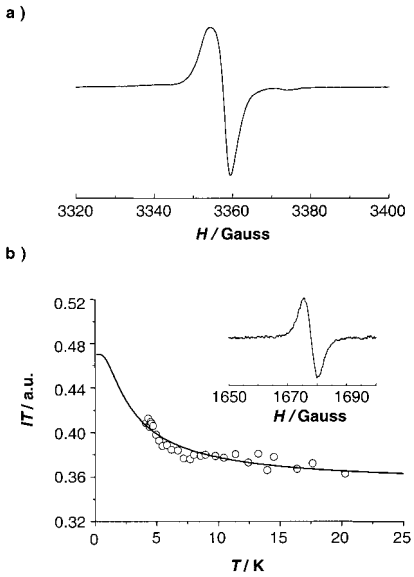

Figure 9. a) Experimental ESR $\Delta m_S = \pm 1$ signal of PTMA at 106 K. Concentration: 5.3×10^{-3} M in CH_2Cl_2/toluene; frequency: 9.406904 GHz; power: 3.212×10^{-2} mW; modulation amplitude: 0.5 G. b) Temperature dependence of the peak–peak intensity, I_{pp}, plotted as $I_{pp}T$ product versus T, which corresponds to the $\Delta m_S = \pm 2$ transition. The solid line is the best fit of the experimental data to the Bleaney–Bowers equation. Inset: Observed $\Delta m_S = \pm 2$ signal at 106 K.

confirm the presence of aggregates in concentrated solutions of radical PTMA, but this result does not permitan assessment of either the nature or the size of such aggregates due to the poorly resolved spectra.

Solid-state studies: The static magnetic susceptibility, χ, of polycrystalline samples of both α and β phases of PTMA as well as of radical NOA, was measured between 5 and 300 K with a SQUID susceptometer. At room temperature, the χT product values for all three samples agree with the theoretical value of 0.375 emu K^{-1} mol^{-1} for uncorrelated $S = 1/2$ moieties. The paramagnetic susceptibility χ of NOA, which is plotted as χT product in Figure 10, decreases when the

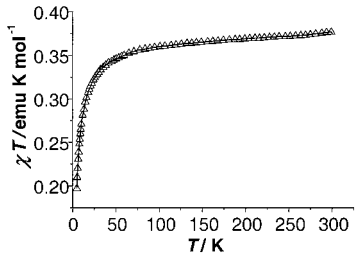

Figure 10. Temperature dependence of the magnetic susceptibility χ of polycrystalline sample of NOA which is plotted as χT versus T. Solid line is the best fit of the experimental data.

temperature is lowered below 50 K. This reveals the presence of dominant antiferromagnetic interactions at low temperature in the solid state. In the crystal structure, through-space contacts between NO groups that bear most of the spin density are longer than 6 Å; this suggests that the major interactions are intradimeric. As described before, the ESR

0947-6539/02/0816-3642 $ 20.00+.50/0 *Chem. Eur. J.* **2002**, *8*, No. 16

studies showed the propagation of weak ferromagnetic interactions within the hydrogen-bonded dimers. Consequently, an additional antiferromagnetic interaction, due to interdimer interactions, competes with the ferromagnetic intradimer interaction, giving rise to the resulting magnetic behavior. Surprisingly, this additional interaction is stronger than the intradimer interaction even when the centers are far apart, and the behavior fitted well to a Curie–Weiss law with $\theta = -4.1$ K. Examination of the crystal structure suggests that the $\pi\cdots\pi$ stacking present between head–tail dimers may be responsible for this strong antiferromagnetic interaction.

The α phase of PTMA exhibits a paramagnetic behavior in the 6–200 K temperature range, and the onset of weak ferromagnetic interactions below 6 K (Figure 11). To confirm

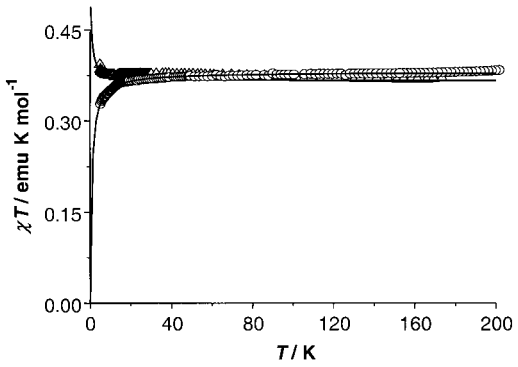

Figure 11. Temperature dependences of the magnetic susceptibility, χ, of polycrystalline samples of α (△) and β (○) phases of radical PTMA which is plotted as χT versus T. Solid lines are the best fit of the experimental data.

this behavior, ESR measurements were performed on an oriented single crystal of the α phase and revealed the same trend. Hence, weak dominant ferromagnetic interactions are present in this phase. The hydrogen-bonded dimers could be responsible, as in the case of NOA, for the appearance of the ferromagnetic interaction within the dimers. As only Cl···Cl contacts are present between the dimers and the distances between them are quite large, it is possible that the dimers behave as magnetically independent species. Therefore, the Bleaney–Bowers equation was used to fit the magnetic data and gave the following exchange coupling constant, $J/k_B = +0.5 \pm 0.1$ K. This value was later confirmed by fitting single-crystal ESR data which gave a similar value, $J/k_B = +1.6 \pm 0.2$ K. In order to validate the ferromagnetic nature of the intradimer interaction, which could not be assessed by ESR measurements in solution, the magnetic data of the β phase was obtained and compared to those of the α phase. Indeed, the β phase differs mainly from the α phase by the absence of such hydrogen-bonded dimers. If these patterns were responsible for the ferromagnetic interaction of the α phase, this ferromagnetic interaction should not be present in the β phase.

The χT product of the β phase of PTMA is plotted against temperature in Figure 11, and shows a continuous decrease as the temperature is lowered. This behavior was fitted to the Curie–Weiss law with a Weiss constant of $\theta = -0.80$ K and indicates of the presence of dominant antiferromagnetic interactions. Cl···Cl contacts may be responsible for this weak antiferromagnetic interaction, as seen in other chlorinated triphenylmethyl radical derivatives.[23] Hence, the comparison of the solid-state magnetic data of both phases clearly showed that the propagation of a ferromagnetic interaction occurs through the hydrogen bond that joins the radicals.

Conclusion

The two open-shell benzoic acid derivatives PTMA and NOA have been used to generate well-defined dimer aggregates in solution, with the aim of investigating whether magnetic exchange occurs at distances longer than 15 Å through noncovalent hydrogen bonds. Such aggregates were found to be present in solution for the NOA radical, and these provided a direct assessment of the resulting ferromagnetic magnetic exchange value. In the case of radical PTMA, aggregates formed through other Cl···Cl and $\pi\cdots\pi$ interactions in solution, as shown by comparison with a reference compound. Indeed, special care must be taken in the study of aggregation and proper reference compounds must be used for each type of radical to ensure that the working concentration does not involve other types of aggregates than those formed through hydrogen bonding. Despite this problem, the exchange interactions were assessed by the consideration of solid-state magnetic behavior. Indeed, the bulkiness of the PTMA radical formed nearly isolated hydrogen-bonded dimers in its α phase. Thus, the exchange interaction through the long-range noncovalent pathway was investigated through solid-state magnetic data and was shown to be ferromagnetic as for NOA. Suppression of this interaction in the β phase, in which dimers were not formed, gave further evidence that the hydrogen-bonded dimers are the species uniquely responsible for this interaction. This magnetic exchange interaction at a long distance is more surprising in this case, since the COOH groups are strongly twisted. Therefore, we have demonstrated that exchange through hydrogen-bonded bridges can occur at a long distance even in the cases of well-delocalized radicals. Even if these noncovalent interactions remain weak, they can play a role in the establishment of ordered magnetic materials when two- and three-dimensional hydrogen-bonded networks are present.

Experimental Section

Materials and methods: Solvents were distilled before use. In particular, THF was dried over sodium/benzophenone, and distilled under Argon. CO_2 gas was dried over concentrated H_2SO_4 and molecular sieves (3 Å). All the reagents were used as received and they were purchased from Aldrich. Thin-layer chromatography (TLC) was performed on aluminum plates coated with Merck Silica gel $60F_{254}$. Microanalyses were performed by the Servei d'Analisi of the Universitat Autònoma de Barcelona. ^{1}H and ^{13}C NMR spectra were recorded on a Bruker ARX300 spectrometer, FT-IR spectra on a Perkin–Elmer Spectrum One spectrometer, UV-visible spectra on a VARIAN Cary 5 instrument, and the MS spectra on a Jeol JMS-DX300 instrument. The ESR spectra were recorded on X-band Bruker spectrometer (ESP-300E). Temperature was measured by a thermocouple introduced inside the tube, 1.5 cm from the bottom.

Magnetic susceptibility measurements were obtained with a Quantum Design SQUID magnetometer. Crystals were measured on a Nonius KappaCCD diffractometer with an area detector and graphite-monochromized $Mo_{K\alpha}$ radiation.

CCDC 175393 (radical NOA), 175394 (α phase, radical PTMA), and 175395 (β phase, radical PTMA) contain the supplementary crystallographic data for this paper. These data can be obtained free of charge via www.ccdc.cam.ac.uk/conts/retrieving.html (or from the Cambridge Crystallographic Data Centre, 12 Union Road, Cambridge CB2 1EZ, UK; fax: (+44) 1223-336-033; or e-mail: deposit@ccdc.cam.ac.uk)..

1-[*N*-*tert*-Butyl-*N*-(*tert*-butyldimethylsiloxy)amino]-4-benzoic acid: A solution of *tert*-butyllithium (8.8 mL of a 1.7 M solution, 15.0 mmol) was added dropwise to 1-[*N*-*tert*-butyl-*N*-(*tert*-butyldimethylsiloxy)amino]-4-bromobenzene[21] (4.88g, 13.7 mmol) in THF (100 mL) at $-80\,^{\circ}C$. The resulting yellow-orange mixture was stirred at this temperature for 1 h and then allowed to warm slowly to room temperature. The mixture was then cooled to $-30\,^{\circ}C$, and CO_2 was bubbled into the vigorously stirred solution until its consumption ceased. The mixture was then acidified with a 2 M HCl solution until pH = 2. After the usual treatment, removal of the solvents yielded 4.1 g of a cream semisolid which was purified by silica column chromatography (dichloromethane) to give 3.8 g of a white microcrystalline solid. Yield: 85 %; ^1H NMR (250 MHz, $CDCl_3$): $\delta = 8.02$ (d, 2H), 7.37 (d, 2H), 1.12 (s, 9H), 0.92 (s, 9H), -0.09 ppm (br s, 6H); MS FAB + (NBA): *m*/*z* (%): 324 (30) [M^++H]; elemental analysis calcd (%) for $C_{17}H_{29}NO_3Si$: C 63.12, H 9.04, N 4.33, Si 8.68; found C 63.16, H 9.10, N 4.29, Si 8.81.

1-[*N*-*tert*-Butyl-*N*-(hydroxyl)amino]-4-benzoic acid: Hydrofluoric acid (0.17 mL, 22 M) was added to a solution of 1-[*N*-*tert*-butyl-*N*-(*tert*-butyldimethylsiloxy)amino]-4-benzoic acid (1.00 g, 3.0 mmol) in THF (10 mL). The mixture was stirred under inert atmosphere for 1 h and then evaporated under vacuum to give 0.60 g of a white powder. Yield 92 %; m.p.: 170 °C (decomp); ^1H NMR (250 MHz, CD_3COCD_3) $\delta = 7.97$ (d, 2H), 7.37 (d, 2H), 1.22 ppm (s, 9H); MS FAB + (NBA): *m*/*z* (%): 210 [M^++H]; IR (KBr) $\tilde{\nu} = 3246$ (s, br, OH), 2971 (s, CH,*t*Bu), 2650 (s, br, OH), 1686, 1606 (s, s, C=O), 1581 cm^{-1} (m, C=CAr); elemental analysis calcd (%) for $C_{11}H_{15}NO_3$: C 63.14, H 7.23, N 6.69; found C 63.11, H 7.15, N 6.78.

1-[*N*-*tert*-Butyl-*N*-(oxyl)amino]-4-benzoic acid: Lead dioxide (1 g) was added to a solution of 1-[*N*-*tert*-butyl-*N*-(hydroxy)amino]-4-benzoic acid (0.5 g, 2.4 mmol) in ethanol (10 mL). The mixture was vigorously stirred for 1 h and then filtered on a glass frit. Evaporation of the solvent gave 0.55 g of a red solid, which was purified by silica chromatography (dichloromethane/ethylacetate 50:50) to give 0.42 g of a red crystalline powder. Yield 84 %; m.p.: 162 – 167 °C (decomp); MS FAB – (NBA): *m*/*z* (%): 207 (100) [M^- – H]; IR (KBr) $\tilde{\nu} = 3116$ (w, CH,Ar), 2978 (m, CH,*t*Bu), 2667, 2558 (m, m, OH), 1675, 1588 (s, s, C=O), 1563 (m, C=CAr), 1430 (s, δ*t*Bu); elemental analysis calcd (%) for $C_{11}H_{14}NO_3$: C 63.45, H 7.78, N 6.73; found C 63.57, H 6.42, N 6.45.

Acknowledgements

This work was supported by grants from the DGI, Spain (Proyecto no. MAT2000-1388-C03-01), Generalitat de Catalunya (2001SGR-00362), the 3MD Network of the TMR program of the E.U. (Contract ERBFMRXCT 980181), ESF Scientific Programme, and the Region Languedoc-Roussillon (Mobility program). We warmly thank Dr. Carlos J. Gómez-García (Universitat de Valencia) for the magnetic susceptibility measurements.

[1] For a general review of the state-of-art of the field: *Magnetic Properties of Organic Materials* (Ed.: P. M. Lahti), Marcel Dekker, New York, **1999**, and references therein.

[2] a) M. Kinoshita, P. Turek, M. Tamura, K. Nozawa, D.Shiomi, Y. Nakazawa, M. Ishikawa, M. Takahashi, K. Awaga, T. Inabe, Y. Maruyama, *Chem. Lett*. **1991**, 1225; b) M. Tamura, Y. Nakazawa, D. Shiomi, K. Nozawa, Y. Hosokoshi, M. Ishikawa, M. Takahashi, M. Kinoshita, *Chem. Phys. Lett*. **1991**, *186*, 401.

[3] a) G. R. Desiraju, *Crystal Engineering: The Crystal as a Supramolecular Entity: Perspectives in Supramolecular Chemistry*, *Vol. 2*, Wiley, New York, **1996**; b) R. Taylor, O. Kennard, *Acc. Chem. Res.* **1984**, *17*, 320; c) J. A. Zerkowski, C. T. Sete, D. A. Wierda, G. M. Whitesides, *J. Am. Chem. Soc.* **1990**, *112*, 9025; d) M. C. Etter, *Acc. Chem. Res.* **1990**, *23*, 120.

[4] T. Otsuka, T. Okuno, K. Awaga, T. Inabe, *J. Mater. Chem*. **1998**, *8*, 1157.

[5] a) T. Akita, Y. Mazakati, K. Kobayashi, *J. Chem. Soc. Chem. Commun.* **1995**, 1861; b) T. Akita, Y. Mazakati, K. Kobayashi, *Mol. Cryst. Liq. Cryst.* **1997**, *306*, 257; c) Y. Pontillon, T. Akita, A. Grand, K. Kobayashi, E. Lelievre-Berna, J. Pécaut, E. Ressouche, J. Schweitzer, *J. Am. Chem. Soc*. **1999**, *121*, 126.

[6] a) E. Hernandez, M. Mas, E. Molins, C. Rovira, J. Veciana, *Angew. Chem.* **1993**, *105* 919; *Angew. Chem. Int. Ed. Engl.* **1993**, *32*, 882; b) J. Cirujeda, L. E. Ochando, J. M. Amigo, C. Rovira, J. Ruis, J. Veciana, *Angew. Chem.* **1995**, *107*, 99; *Angew. Chem. Int. Ed. Engl.* **1995**, *34*, 55; c) J. Cirujeda, M. Mas, E. Molins, F. Lanfranc de Panthou, J. Laugier, J. G. Park, C. Paulsen, P. Rey, C. Rovira, J. Veciana, *J. Chem. Soc. Chem. Commun*. **1995**, 709; d) J. Cirujeda, E. Hernandez-Gasio, C. Rovira, J.-L. Stanger, P. Turek, J. Veciana, *J. Mater. Chem.* **1995**, *5*, 243; e) J. Veciana, J. Cirujeda, C. Rovira, E. Molins, J. J. Novoa, *J. Phys.* **1996**, 1967; f) T. Sugawara, M. Matsushita, A. Izuoka, N. Wada, N. Takeda, M. Ishikawa, *J. Chem. Soc. Chem. Commun.* **1994**, 1723; f) M. Matsuchida, A. Izuoka, T. Sugawara, T. Kobayashi, N. Wada, N. Takeda, M. Ishikawa, *J. Am. Chem. Soc.* **1997**, *119*, 4369; g) J. Cirujeda, PhD Thesis, Universitat Ramon Llull, **1997**.

[7] T. Akita, K. Kobayashi, *Adv. Mater.* **1997**, *9*, 346.

[8] a) N. Yoshioka, M. Irisawa, Y. Mochizuki, T. Kano, H. Inoue, S. Ohba, *Chem. Lett*. **1997**, 251; b) N. Yoshioka, M. Irisawa, Y. Mochizuki, T. Aoki, H. Inoue, *Mol. Cryst. Liq. Cryst.* **1997**, *306*, 403.

[9] J. R. Ferrer, P. M. Lahti, C. George, G. Antonerra, F. Palacio, *Chem. Mater*. **1999**, *8*, 205.

[10] A. Lang, Y. Pei, L. Ouahab, O. Kahn, *Adv. Mater.* **1996**, *8*, 60.

[11] R. Feher, D. B. Amabilino, K. Wurst, J. Veciana, *Mol. Cryst. Liq. Cryst.* **1999**, *334*, 333.

[12] L. Catala, R. Feher, D. B. Amabilino, K. Wurst, J. Veciana, *Polyhedron*, **2001**, *20*, 1571.

[13] a) F. M. Romero, R. Ziessel, A. De Cian, J. Fischer, P. Turek, *New J. Chem*. **1996**, *20*, 919; b) F. M. Romero, R. Ziessel, M. Drillon, J.-L. Tholence, C. Paulsen, N. Kyritsakas, J. Fischer, *Adv. Mater.* **1996**, *8*, 826; c) F. M. Romero, R. Ziessel, M. Bonnet, Y. Pontillon, E. Ressouche, J. Schweitzer, B. Delley, A. Grand, C. Paulsen, *J. Am. Chem. Soc*. **2000**, *122*, 1298.

[14] a) C. Stroh, F. M. Romero, N. Kyritsakas, L. Catala, P. Turek, R. Ziessel, *J. Mater. Chem*. **1999**, *9*, 875; b) O. Felix, M. W. Hosseini, A. De Cian, J. Fischer, L. Catala, P. Turek, *Tetrahedron Lett.* **1999**, *40*, 2943.

[15] G. A Jeffrey, W. Saenger, *Hydrogen Bonding in Biological Structures*, Springer, Berlin **1994**.

[16] C. Ikeda, N. Nagahara, E. Motegi, N. Yoshioka, H. Inoue, *Chem. Commun.* **1999**, 1759.

[17] K. Inoue, H. Iwamura, *Chem. Phys. Lett*. **1993**, *207*, 551.

[18] N. C. Schiødt, F. Fabrizi de Biani, A. Caneschi, D. Gatteschi, *Inorg. Chim. Acta* **1996**, *248*, 139.

[19] V. Laget, C. Hornick, P. Rabu, M. Drillon, P. Turek, R. Ziessel, *Adv. Mater.* **1998**, *10*, 1024.

[20] a) K. Inoue, H. Iwamura, *Angew. Chem.* **1995**, *107*, 973; *Angew. Chem. Int. Ed. Engl.* **1995**, *34*, 927; b) D. A. Schultz, A. K. Boal, *Mol. Cryst. Liq. Cryst*. **1995**, *272*, 75.

[21] M. Ballester, J. Castañer, J. Riera, A. Ibáñez, J. Pujades, *J. Org. Chem.* **1982**, *47*, 259.

[22] B. Kariuki, C. L. Bauer, K. D. M. Harris, S. J. Teat, *Angew. Chem.* **2000**, *112*, 4659; *Angew. Chem. Int. Ed.* **2000**, *39*, 24, 4485.

[23] a) O. Armet, J. Veciana, C. Rovira, J. Riera, J. Castañer, E. Molins, J. Rius, C. Miravitlles, S. Olivella, J. Brichfeus, *J. Phys. Chem.* **1987**, *91*, 5608; b) J. Sedó, N. Ventosa, M. A. Molins, M. Pons, C. Rovira, J. Veciana, *J. Org. Chem.* **2001**, *66*, 1567.

[24] a) D. A. Shultz, K. P. Gwaltney, H. Lee, J. *Org. Chem.* **1998**, *63*, 769; b) G. Barbarella, A. Rassat, *Bull. Soc. Chim. Fr.* **1969**, 2378.

[25] a) R. Brière, R.-M. Dupeyre, H. Lemaire, C. Morat, A. Rassat, P. Rey, *Bull. Soc. Chim. Fr.* **1965**, 3290; b) J. E. Wertz, J. R. Bolton, *Electron*

  0947-6539/02/0816-3644 $ 20.00+.50/0

spin Resonance, Elementary Theory and Practical Applications, **1994**, Chapman and Hall, New York, p. 112.
[26] W. B. Gleason, R. E. Barnett, *J. Am. Chem. Soc.* **1976**, *98*, 2701.
[27] S. S. Eaton, K. M. More, B. M. Sawant, G. R. Eaton, *J. Am. Chem. Soc.* **1983**, *105*, 6560.
[28] A. A. Dubinskii, O. Ya. Grinberg, A. A. Tabachnik, V. P. Ivanoo, E. G. Rozantzev, Ya. S. Lebedev, *Biofizika* **1974**, *19*, 840.
[29] B. Bleaney, K. D. Bowers, *Proc. R. Soc. London Ser. A* **1952**, *214*, 451.
[30] M. Ballester, J. Riera, J. Castañer, C. Badía, J. M. Monsó, *J. Am. Chem. Soc.* **1971**, *93*, 2215.
[31] D. Ruiz-Molina, PhD Thesis, Universitat Autónoma de Barcelona, Spain, **1995**.

Received: December 4, 2001 [F3722]

  0947-6539/02/0816-3645 $ 20.00+.50/0

Article B

Títol: A robust nanocontainer based on a pure organic free radical.

Autors: D. Maspoch, N. Domingo, D. Ruiz-Molina, K. Wurst, J. Tejada, C. Rovira, J. Veciana.

Publicació: J. Am. Chem. Soc. 2004, 126, 730.

(No presentat a la Comissió de Doctorat).

J|A|C|S
COMMUNICATIONS

Published on Web 01/03/2004

A Robust Nanocontainer Based on a Pure Organic Free Radical

Daniel Maspoch,[†] Neus Domingo,[‡] Daniel Ruiz-Molina,[†] Klaus Wurst,[§] Javier Tejada,[‡] Concepció Rovira,[†] and Jaume Veciana*,[†]

Institut de Ciència dels Materials de Barcelona (CSIC), Campus UAB, 08193, Cerdanyola, Catalonia, Spain, Facultat de Física, Universitat de Barcelona, Diagonal 647, 08028-Barcelona, Spain, and Institut für Allgemeine, Anorganische und Theoretische Chemie, Universität Innsbruck, Innrain 52a, A-6020, Innsbruck, Austria

Received October 10, 2003; E-mail: vecianaj@icmab.es

Proper supramolecular self-assembly of organic molecules in the solid state is one of the most important challenges for the development of multifunctional molecular materials.[1] Among them, recently much more effort has been focalized toward the obtaining of magnetic nanoporous materials. Indeed, thus far several metal-organic open-framework structures that combine the inherent characteristics of nanoporous materials and the occurrence of magnetic exchange interactions between transition metal ions have been obtained.[2,3] However, even though several examples of pure organic nanoporous systems have already been described,[4,5] to the best of our knowledge, none of them exhibit magnetic properties due to the lack of transition-metal ions and the diamagnetic character of the organic molecular bricks used thus far. Herein, we present the first example of a purely organic magnetic and robust nanoporous lattice based on the supramolecular arrangement of an open-shell molecule, the dicarboxylic perchlorinated triphenylmethyl (PTM) radical **1**. The use of this free radical as a supramolecular synthon has several advantages:[6] (1) radical **1** exhibits a high thermal and chemical stability, (2) its trigonal symmetry provides a typical template for getting channels held together by hydrogen bonds through the two carboxylic groups, (3) the molecular bulkiness and rigidity of PTM radicals is expected to prevent close packing of molecular units, and (4) besides their structural control, hydrogen bonds have also been shown to favor magnetic exchange interactions between bound organic radical molecules.[7] Crystallization of the dicarboxylic radical **1**[8] generates the pure organic radical open-framework (POROF-1) material, combining large hydrophobic nanocavities with hydrophilic windows along with magnetic characteristics.

Radical **1** was prepared following a new three-step procedure, starting from compound **2**.[9] Dichloromethyl groups were introduced by reacting **2** with chloroform following a Friedel−Crafts reaction using $AlCl_3$ as catalyst (78%) and subsequently were converted to carboxylic groups by a hydrolysis-oxidation reaction using oleum 20% (31%). Finally, the subsequent treatment of the hydrocarbon precursor **4** with excess of NaOH, I_2, and HCl gave radical **1** (90%). Single crystals of POROF-1, suitable for X-ray diffraction, were obtained by a diffusion of *n*-hexane into a solution of **1** in dichloromethane.[9]

Radical **1** crystallizes in a trigonal *R*-3 space group with 18 molecules of radical **1** packed in the unit cell. Molecular arrangement of **1** creates a primary structure consisting of two-dimensional hydrogen-bonded sheets along the *ab* plane, where each molecule of **1** participates in the construction of two different hydrogen-bonded motifs. The repetitive unit consists of an unusual hexamer of radicals hydrogen-bonded through one carboxylic group [R_6^6 (24)], with bond distances of 1.837 Å and bond angles of 168.5° (Figure 1). The second carboxylic group of each radical acts as a connecting element between hexameric units by the formation of

Scheme 1

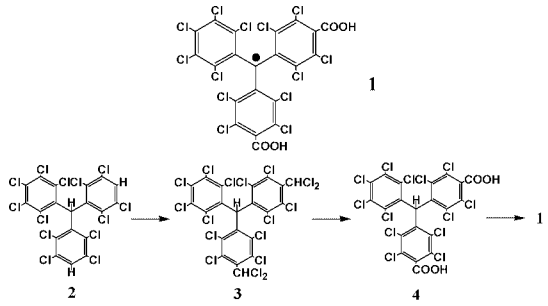

two complementary hydrogen bonds between two carboxylic groups [R_2^2 (8)], with a bond distance of 1.865 Å and bond angle of 163.2°.[11] In this way, each hexamer is linked with six more identical units in an hexagonal topology, extending the infinitely hydrogen-bonded net along the *ab* plane (Figure 1). Further supramolecular interactions, in particular four H-bonds between chlorine atoms and carboxylic groups and six Cl···Cl contacts per molecule,[12] contribute to an additional stabilization of the hydrogen-bonded network.

A view down the *c* axis of the crystal structure of POROF-1 reveals a stacking of laterally shifted layers held together through several Cl···Cl contacts (Figure 2), yielding an ABCABC arrangement. The packing of these pillared sheets leads a pure organic open-framework structure with one-dimensional nanochannels formed by narrowed polar windows and larger hydrophobic cavities. Indeed, as illustrated in Figure 2, these channels contain large hydrophobic nanocavities where a sphere 10 Å in diameter can fit inside them and smaller windows with a highly hydrophilic environment due to the presence of the carboxylic groups at the inner rims. The diameter of such hydrophilic windows is 5 Å, considering van der Waals radius. The unusual combination of connected nanocavities and windows gives way to solvent-accessible voids in the crystal structure that amount to 31% (5031 $Å^3$ per unit cell) of the total volume (16 158 $Å^3$).[13]

To evaluate the structural robustness of POROF-1, we have examined, by a combination of thermal gravimetric analysis and X-ray powder diffraction (XRPD) experiments, an as-synthesized crystalline sample of POROF-1.[14] In the as-synthesized material, the large hydrophobic cavities are occupied by six *n*-hexane solvate molecules (one molecule of *n*-hexane per one molecule of radical **1**). Accordingly, when an as-synthesized sample of POROF-1 was heated to 100 °C, a weight loss of 9%, ascribed to the complete loss of all guest *n*-hexanes molecules, was observed. Such a loss was confirmed by complementary elemental analysis. Beyond this temperature, thermal analysis does not exhibit any significant change up to 275 °C, whereupon an abrupt weight loss attributed to the decomposition of **1** was observed. Simultaneously, XRPD studies confirmed that POROF-1 remains crystalline and stable up to 275 °C. Indeed, the XRPD pattern of a sample that was heated

[†] Institut de Ciència dels Materials de Barcelona.
[‡] Universitat de Barcelona.
[§] Universität Innsbruck.

10.1021/ja038988v CCC: $27.50

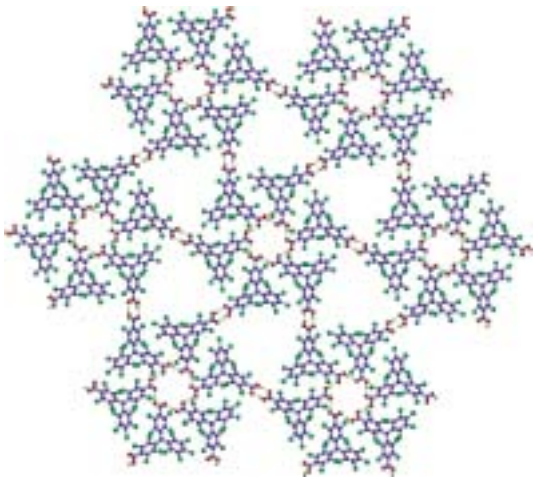

Figure 1. Crystal structure of POROF-1. Two-dimensional hydrogen-bonded layer. Within one layer, the repetitive $R_6^6(24)$ H-bonded hexamer originates a polar window due to the presence of six carboxylic groups, whereas linking of each hexamer with six more identical units in an hexagonal topology originates six trigonal-shaped hydrophobic voids.

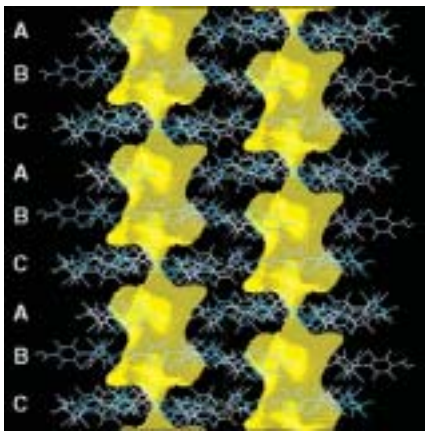

Figure 2. Space-filling view along the *b* axis of the large nanocontainers formed along the one-dimensional channel.

at 265 °C shows that the positions and intensities of all lines remain unchanged when compared with the XRPD pattern of an as-synthesized sample. Such a thermal stability is highly remarkable and comparable to those observed for other stable supramolecular systems, such as multi H-bonded aggregates derived from the cyanuric acid and melamine.[15]

Variable temperature magnetic susceptibility data for an as-synthesized crystalline sample of POROF-1 were obtained on a SQUID magnetometer, under a temperature range of 1.8−300 K. POROF-1 exhibits a paramagnetic behavior in the 50−300 K temperature range, with a $\chi \cdot T$ product value of 0.385 emu K mol^{-1} at 300 K, that fully agrees with the theoretical value of 0.375 emu K mol^{-1} expected for an uncorrelated spin ($S = 1/2$). Below 50 K, the $\chi \cdot T$ value decreases upon decreasing temperature, consistently with the presence of weak intermolecular antiferromagnetic interactions. This magnetic behavior remains constant in the absence of guest solvent molecules.

In summary, self-assembly of radical **1** generates a paramagnetic open-framework structure with one-dimensional nanochannels formed by narrowed polar windows and large hydrophobic nanocontainers. Moreover, POROF-1 is one of the scarce examples of pure organic porous materials that remains stable up to 275 °C, even after removal of internal solvate guest molecules.[16] Such structural features, joined to its solubility in polar organic solvents, give to POROF-1 the possibility to be a good candidate for future ship-in-bottle synthesis applications.[17] Further studies to validate the use of polycarboxylic organic radicals as building blocks for obtaining pure organic magnetic nanoporous molecular materials are currently underway.

Acknowledgment. We thank the Programa Nacional de Materiales (MAT2003-04699) and DGR, Catalunya (2001SGR00362). D.M. thanks the Generalitat de Catalunya for a predoctoral grant.

Supporting Information Available: Crystallographic data, thermal gravimetric analysis, and XRPD patterns and magnetic properties of POROF-1 (PDF, CIF). This material is available free of charge via the Internet at http://pubs.acs.org.

References

(1) (a) *Supramolecular Chemistry*, Lehn, J. M., Ed., VCH: Weinheim, Germany, 1995. (b) Aakeröy, C. B.; Beatty, A. M.; Helfrich, B. A. *Angew. Chem., Int. Ed.* **2001**, *40*, 3240.

(2) For recent examples on metal-organic open frameworks, see: (a) Chen, B.; Eddaoudi, M.; Hyde, S. T.; O'Keefe, M.; Yaghi, O. M. *Science* **2001**, *291*, 1021. (b) Noro, S. I.; Kitagawa, S.; Kondo, M.; Seki, K. *Angew. Chem., Int. Ed.* **2000**, *12*, 2081.

(3) For recent examples on magnetic metal-organic open frameworks, see: (a) Maspoch, D.; Ruiz-Molina, D.; Domingo, N.; Wurst, K.; Cavallini, M.; Biscarini, F.; Tejada, J.; Rovira, C.; Veciana, J. *Nat. Mater.* **2003**, *2*, 195. (b) Beauvais, L. G.; Long, J. R. *J. Am. Chem. Soc.* **2002**, *124*, 12096. (c) Barthelet, K.; Marrot, J.; Riou, D.; Férey, G. *Angew. Chem., Int. Ed.* **2002**, *41*, 281. (d) Moulton, B.; Lu, J.; Hajndl, R.; Hariharan, S.; Zaworotko, M. J. *Angew. Chem., Int. Ed.* **2002**, *41*, 2821. (e) Price, D. J.; Tripp, S.; Powell, A. K.; Wood, P. T. *Chem.−Eur. J.* **2001**, *7*, 200. (f) Chui, S. S.-Y.; Lo, S. M.-F.; Charmant, J. P. H.; Orpen, A. G.; Williams, I. D. *Science* **1999**, *283*, 1148.

(4) For recent reviews on organic nanoporous open-framework materials, see: (a) Nangia, A. *Curr. Opin. Solid State Mater. Sci.* **2001**, *5*, 115. (b) Zaworotko, M. J. *Angew. Chem., Int. Ed.* **2000**, *39*, 3052. (c) Langley, P. J.; Hulliger, J. *Chem. Soc. Rev.* **1999**, *28*, 279. (d) Desiraju, G. R. *Curr. Opin. Solid State Mater. Sci.* **1997**, *2*, 451.

(5) For recent examples on organic open-framework materials, see: (a) Miyahara, Y.; Abe, K.; Inazu, T. *Angew. Chem., Int. Ed.* **2002**, *41*, 3020. (b) Bong, D. T.; Ghadiri, M. R. *Angew. Chem., Int. Ed.* **2001**, *40*, 2163. (c) Sada, K.; Sugahara, M.; Kato, K.; Miyata, M. *J. Am. Chem. Soc.* **2001**, *123*, 4386. (d) Müller, T.; Hulliger, J.; Seichter, W.; Weber, E.; Weber, T.; Wübbenhorst, M. *Chem.−Eur. J.* **2000**, *6*, 54. (e) Kobayashi, K.; Shirasaka, T.; Sato, A.; Horst, E.; Furukawa, N. *Angew. Chem., Int. Ed.* **1999**, *38*, 3483. (f) Biradha, K.; Dennis, D.; MacKinnon, V. A.; Sharma, C. V. K.; Zaworotko, M. J. *J. Am. Chem. Soc.* **1998**, *120*, 11894. (g) Russel, V. C.; Evans, C. C.; Li, W.; Ward, M. D. *Science* **1997**, *276*, 575.

(6) For recent reviews on magnetism of organic materials, see: (a) *Magnetic Properties of Organic Materials*, Lahti, P. M., Ed.; Marcel Dekker: New York, 1999. (b) Veciana, J.; Iwamura, H. *MRS Bull.* **2000**, *25*, 41. (c) *Magnetism: Molecules to Materials*; Miller, J. S.; Drillon, M., Eds.; Wiley-VCS: Weinheim, Germany, 2001; Vols 1−3.

(7) Domingo, V. M.; Castañer, J.; Riera, J.; Labarta, A. *J. Org. Chem.* **1994**, *59*, 2604.

(8) Maspoch, D.; Gerbier, P.; Catala, L.; Vidal-Gancedo, J.; Wurst, K.; Rovira, C.; Veciana, J. *Chem.−Eur. J.* **2002**, *8*, 3635.

(9) Ballester, M.; Riera, J.; Castañer, J.; Rovira, C.; Armet, O. *Synthesis* **1986**, 64.

(10) X-ray structure analysis. Crystal data: $C_{21}H_2Cl_{13}O_4 \cdot C_6H_{14}$, trigonal, space group *R*-3, $a = 31.4651(6)$ Å, $b = 31.4651(7)$ Å, $c = 18.8447(7)$ Å, $V = 16157.6(8)$ Å^3, $Z = 18$, $T = 233(2)$ K, λ-Mo Kα = 0.7173 Å, $F(000) = 7758$, $\mu = 1.032$ mm^{-1}, ρcalcd = 1.601 g/cm^3, red prism 0.15 × 0.08 × 0.08 mm^3. Data collection: Nonius Kappa CCD, 19 275 measured reflections were corrected with the program SCALEPACK. Structure solution and refinement: anisotropic refinement on F2 (SHELXL 97), hydrogens of the acid groups were refined with isotropic parameters; *R*-values for 421 parameters and 2592 observed reflections [$I > 2\sigma(I)$] R1 = 0.0461 and wR2 = 0.1183.

(11) Similar hydrogen-bonded dimers were observed in the monocarboxylic perchlorotriphenylmethyl radical; see ref 7. In this case, bond distance and angle are 1.955 Å and 144°, respectively.

(12) (a) Sarma, J. A. R. P.; Desiraju, G. R. *Acc. Chem. Res.* **1986**, *19*, 222. (b) Desiraju, G. R.; Parthasarathy, R. *J. Am. Chem. Soc.* **1989**, *111*, 8725.

(13) Spek, A. L. *PLATON*, A Multipurpose Crystallographic Tool; Utrecht University: Utrecht, The Netherlands, 1998.

(14) Thermal gravimetric analyses were done with as-synthesized microcrystals of radical **1** which were heated to 350 °C at a constant rate of 3 °C/min.

(15) Whitesides, G. M.; Simanek, E. E.; Mathias, J. P.; Seto, C. T.; Chin, D. N.; Mammen, M.; Gordon, D. M. *Acc. Chem. Res.* **1995**, *28*, 37.

(16) There are only four examples of pure organic open-framework materials remaining structurally ordered when the guest molecules are removed: (a) Sozzani, P.; Comotti, A.; Simonutti, R.; Meersman, T.; Logan, J. W. *Angew. Chem., Int. Ed.* **2002**, *39*, 2695. (b) Brunet, P.; Simard, M.; Wuest, J. D. *J. Am. Chem. Soc.* **1997**, *119*, 2737. (c) Ung, A. T.; Gizachew, D.; Bishop, R.; Scudder, M. L.; Dance, I. G.; Craig, D. C. *J. Am. Chem. Soc.* **1995**, *117*, 8745. (d) Ibragimov, B. T.; Talipov, S. A. *J. Inclusion Phenom. Mol. Recognit.* **1994**, *17*, 317.

(17) There is a previous example of a metal-organic open-framework material suitable for ship-in-bottle synthesis: Pan, L.; Liu, H.; Lei, X.; Huang, X.; Olson, D. H.; Turro, N. J.; Li, J. *Angew. Chem., Int. Ed.* **2003**, *42*, 542.

JA038988V

Supporting Information

A Robust Nanocontainer based on a Pure Organic Free Radical

Daniel Maspoch, Neus Domingo, Daniel Ruiz-Molina, Klaus Wurst, Javier Tejada, Concepció Rovira, and Jaume Veciana*

Institut de Ciència dels Materials de Barcelona (CSIC), Campus UAB, 08193, Cerdanyola, Catalonia, Spain, Facultat de Física, Universitat de Barcelona, Diagonal 647, 08028-Barcelona, Spain, and Institut für Allgemeine, Anorganische und Theoretische Chemie, Universität Innsbruck, Innrain 52a, A-6020, Innsbruck, Austria.

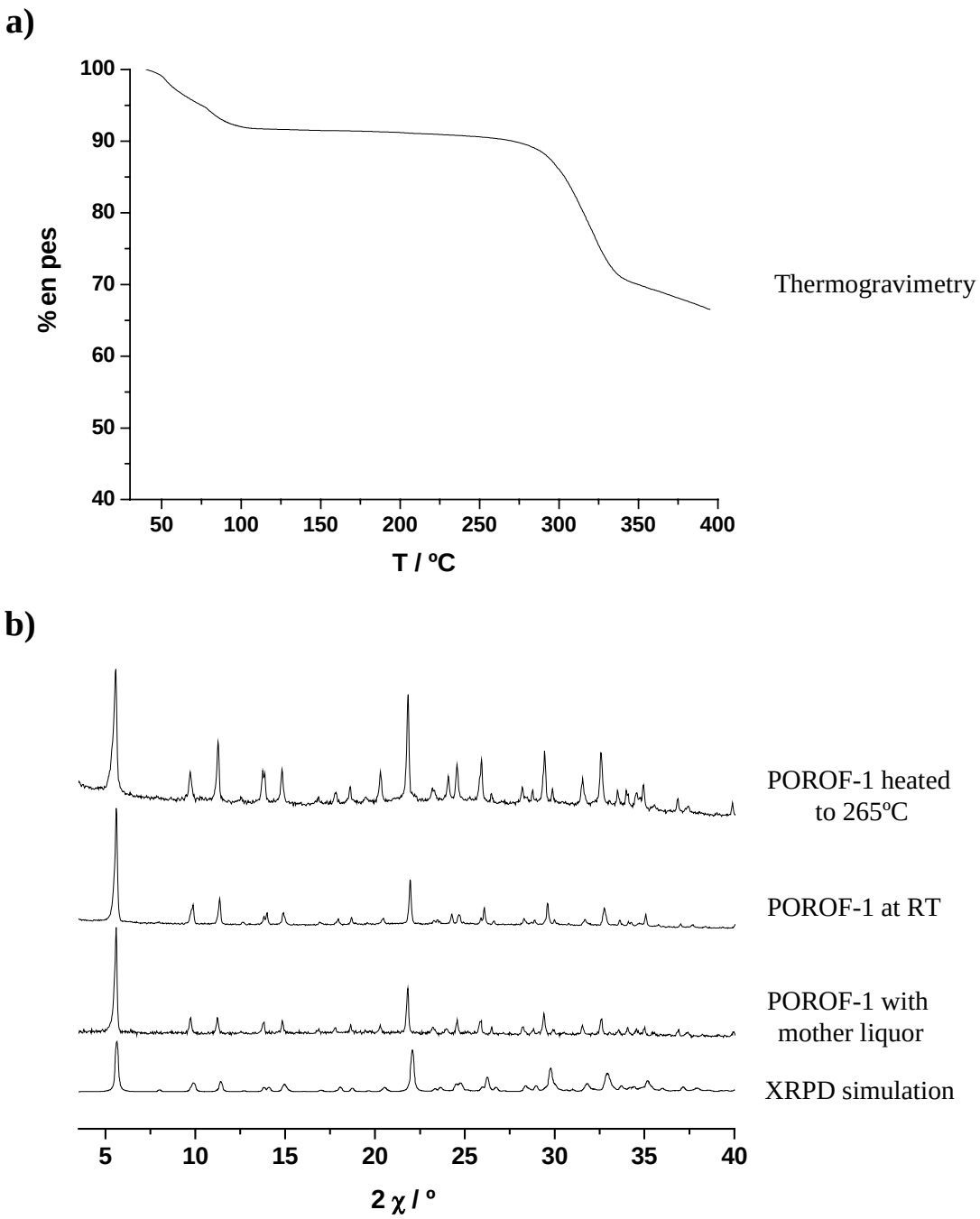

Figure S1 a) Thermogravimetric analysis of POROF-1, under dynamic conditions at a constant rate of 3ºC/min. b) X-ray powder diffractograms of samples of POROF-1, before and after thermal treatments. Below is the simulated pattern obtained from the X-ray single crystal data.

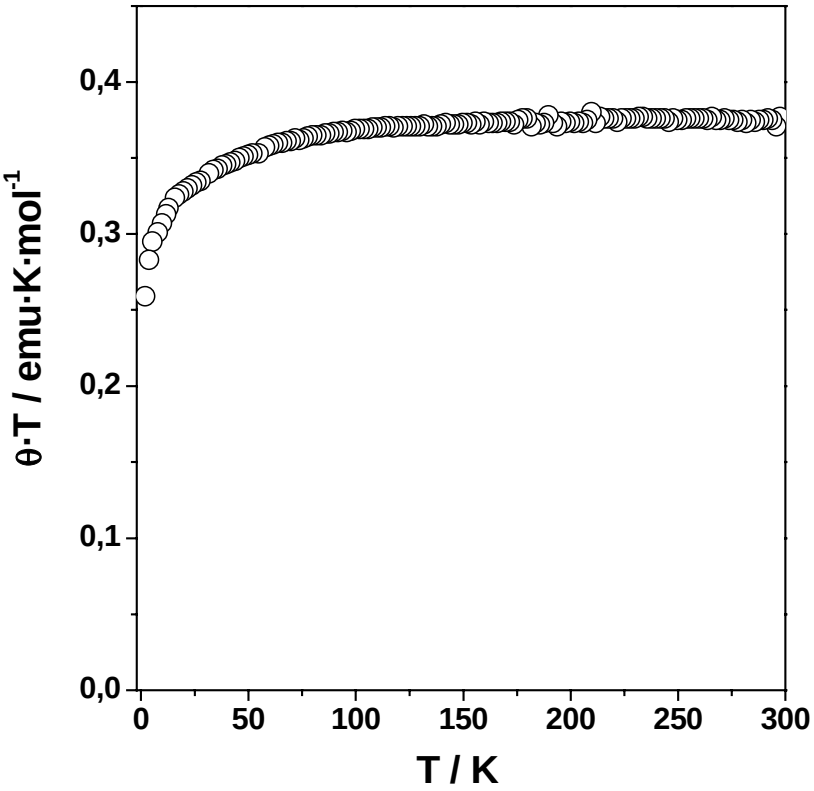

Magnetic properties

Figure S2 Temperature dependence of the magnetic susceptibility of POROF-1.

Article C

Títol: A new robust pure organic nanoporous magnet

Autors: D. Maspoch, N. Domingo, D. Ruiz-Molina, K. Wurst, G. Vaughan, J. Tejada, C. Rovira, J. Veciana.

Publicació: Angew. Chem. Int. Ed., en premsa.

(No presentat a la Comissió de Doctorat)

Magnetic Materials

A Robust Purely Organic Nanoporous Magnet**

*Daniel Maspoch, Neus Domingo, Daniel Ruiz-Molina, Klaus Wurst, Gavin Vaughan, Javier Tejada, Concepció Rovira, and Jaume Veciana**

■■Title ok? we try to avoid words such as New, Novel, etc in titles■■In the last few years, the construction of purely organic-molecule-based magnetic materials has become a topic of interest.[1] Since the first organic ferromagnet was discovered in 1991,[2] a number of other purely organic radicals exhibiting bulk ferromagnetic ordering at very low temperatures (generally below 1.5 K) have been found.[3] For this property to be achieved, synthetic tailoring of open-shell building blocks that allow both a proper control over their supramolecular assembly and the establishment of correct magnetic interactions, are required. Crystal engineering through hydrogen-bonding interactions is a powerful method for achieving both conditions. From a structural point of view, the directional and often predictive nature of hydrogen bonds may allow control of the long-range supramolecular order in solid state.[4] Besides their structural control, hydrogen bonds have also been shown to favor magnetic exchange interactions between bound radical molecules of α-nitronyl nitroxides, α-imino nitroxide, or *tert*-butyl nitroxide derivatives.[5] For instance, attempts to control packing, and therefore magnetic ordering, in phenyl nitronyl aminoxyl radicals substituted by one or two OH groups have been carried out.[6] However, even though efforts on this

[*] D. Maspoch, Dr. D. Ruiz-Molina, Dr. C. Rovira, Prof. J. Veciana
Institut de Ciència de Materials de Barcelona (CSIC)
Campus Universitari de Bellaterra
08193 Cerdanyola (Spain)
Fax: (+34) 3-580-5729
E-mail: vecianaj@icmab.es

N. Domingo, Prof. J. Tejada
Facultad de Física
Universitat de Barcelona
Diagonal 647, 08028 Barcelona (Spain)

Dr. K. Wurst
Institut für Allgemeine, Anorganische und Theoretische Chemie
Universität Innsbruck
Innrain 52a, 6020 Innsbruck (Austria)

Dr. G. Vaughan
European Syncrotron Radiation Facility (E.S.R.F.)
B. P. 220, 38043 Grenoble cedex (France)

[**] This work was supported by Programa Nacional de Materiales of the Dirección General de Investigación (Spain), under project MAT2003-04699, the 3MD Network of the TMR program of the E.U. (contract ERBFMRXCT80181) and Generalitat de Catalunya (2001SGR00362). We thank also Acción Integrada Hipano-Austríaca HU20020046. D.M. is grateful to the Generalitat de Catalunya for a predoctoral grant. N.D. is grateful to the Ministerio de Educación, Cultura y Deportes for a predoctoral grant of the FPU program.

Supporting information for this article is available on the WWW under http://www.angewandte.org or from the author.

direction have been undertaken by different groups, the ultimate design of high-level structures with a ferromagnetic macroscopic behavior must be left in most cases to serendipity, as additional, undesirable intermolecular interactions compete in the solid state.

To circumvent such inconvenience, we have initiated an approach based on the synthesis and study of perchlorotriphenylmethyl (PTM) radicals functionalized with carboxylic groups. PTM radicals, in addition to eminent thermal and chemical stabilities,[7] are bulky molecules which minimize additional through-space intermolecular magnetic interactions.

We have already described the supramolecular arrangement of the monocarboxylic radical **1**.[8] In the solid state radical **1** formed hydrogen-bonded dimers that promoted the transmission of a weak ferromagnetic interaction. Herein we report the supramolecular arrangement and magnetic characterization of the new radical **2** (PTMTC), which offers a

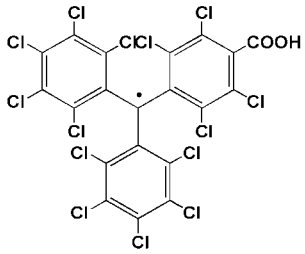

1

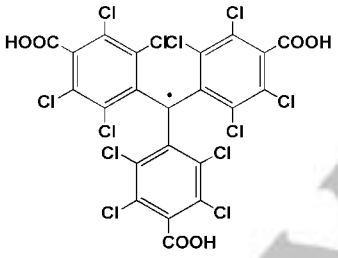

2

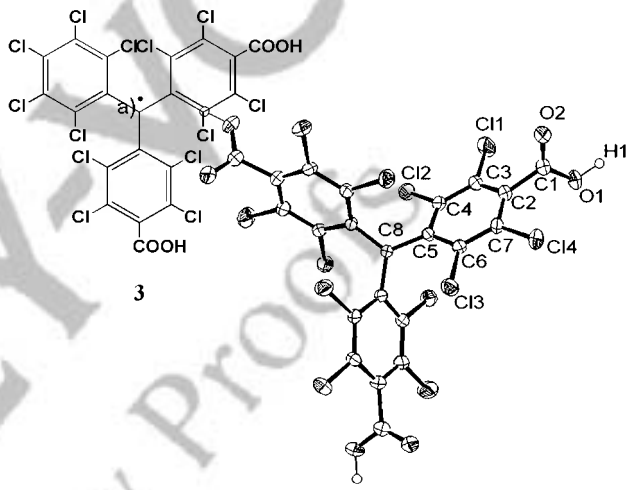

3

rational mechanism to expand the structural, and hence, the magnetic dimensionality of the supramolecular architecture owing to the presence of three carboxylic groups, which are able to form hydrogen bonds. Furthermore, from a strict structural point of view, radical **2**, by analogy with trimesic acid,[9] is expected to generate an open-framework nanoporous structure, a goal within the crystal-engineering field.[10,11] An example of purely organic-radical open-framework (POROF-1), with dominant antiferromagnetic interactions has been obtained by the self-assembly of the dicarboxylic radical **3**.[12] The hydrogen-bonded assembly (named POROF-2) generated from radical **2** has the advantages associated with both mono- and biscarboxylic PTM radicals, it has a robust porous extended network and an architecture that not only combines the presence of highly polar nanotubular channels but also magnetic ordering at low temperatures.

Hexagonal single-crystals of POROF-2 suitable for X-ray diffraction were grown from a mixture of dichloromethane and *n*-hexane. Radical **2** crystallizes on a trigonal $P\bar{3}c1$ space group with four molecules of **2** packed in the unit cell.[13] The high molecular symmetry of the crystal lattice is reflected by the presence of a C_3 symmetry axis that passes through the central carbon (C8) of the radical (see Figure 1a) Thus, the three polychlorinated aromatic rings of radical **2** are identical. Owing to the steric hindrance of the chlorine atoms in *ortho* positions of the phenyl groups, the carboxylic group is twisted by 87° with respect to the plane of the phenyl group to which it is bonded.

Figure 1: Crystal structure of POROF-2. a) ORTEP plot, thermal ellipsoids set at 50% probability, and b) hydrogen-bonded hexamer.

The molecular arrangement of such crystalline radical building blocks creates a primary structure consisting of two-dimensional hydrogen-bonded layers along the *ab* plane. The repeating unit consists of a nontypical hexameric $R_6^6(24)$ hydrogen-bonded motif formed by six molecules of **2** the three-bladed-propeller-like substructures have alternating plus and minus helicities (see Figure 1b)■■ok?■■. In this motif, each radical is hydrogen-bonded to two neighboring radicals through one carboxylic group, with bond lengths of 1.70 Å and bond angles of 169°. Since every radical unit contains three carboxylic groups, each PTMTC molecule participates in the construction of three identical hexameric units that propagate along the *ab* plane (see Figure 2a).

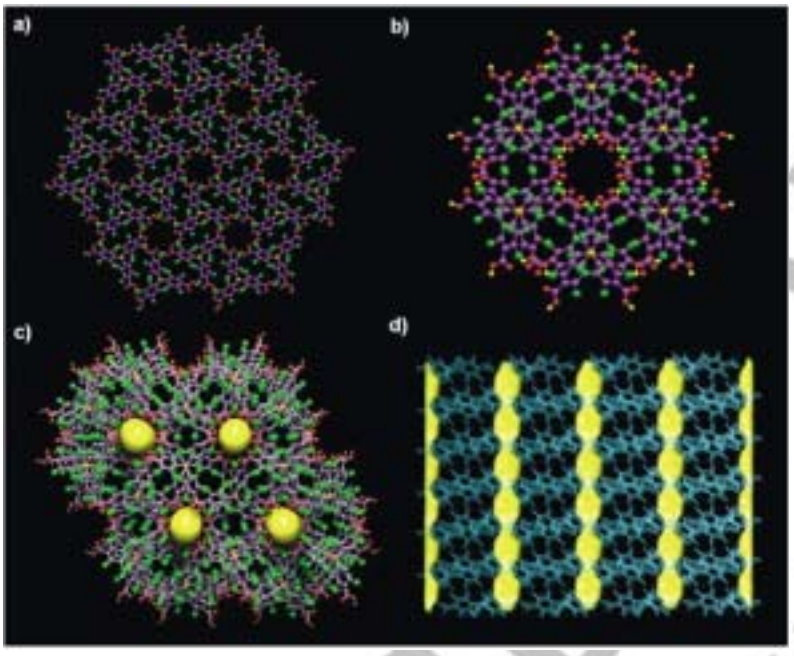

Figure 2: Crystal packing of POROF-2. a) Open-framework network in *ab* plane, b) tubular nanochannel, c) pore view along the *c* axis, the large yellow sphere indicates the dimensions of the tublular channels, and d) pore view along the *a* axis, showing the tubular channels. C violet or orange; O red; Cl green; H yellow. In (a)–(c) the carbon atoms in orange have most of the spin density of radical **2**.

Several chlorine–chlorine contacts (twelve per molecule) between neighboring layers have significant implications for the rigidity of this porous framework, in particular for the secondary structure of POROF-2 that consists of the stacking of different layers with an ABAB alternation along the *c* axis.[14] Surprisingly, the stacking of layers along the *c* axis generates a three-dimensional structure that has tubular channels, into which a sphere 5.2 Å in diameter can fit (see Figure 2b,c). In addition, such nanochannels are surrounded by a second set of small pores with a diameter of 3.3 Å. The combination of both sets of channels gives solvent-accessible voids in the crystal structure that amount to up to 15% (450 $Å^3$ per unit cell) of the total volume.[15] The significant steric congestion caused by the large number of bulky chlorine atoms, can be ascribed as the main reason for obtaining this noncatenated crystal packing.[16]

As can be observed more in detail in Figure 2b, the location of carboxylic groups at the inner walls of the largest

channels furnish these pores with a highly polar and hydrophilic environment. This arrangement may account for the lack of guest solvent molecules (*n*-hexane and/or CH_2Cl_2) within the nanochannels, a situation confirmed not only by X-ray crystallography but also by thermogravimetric studies and elemental analysis. Thermogravimetric analysis of a few single crystals of radical **2** showed no weight loss in the temperature range 25–300 °C, in fact POROF-2 remains crystalline and stable up to 300 °C. Indeed, the powder X-ray diffraction pattern of a sample that was heated up to 300 °C shows that the positions and intensities of all lines remain unchanged when compared with the powder X-ray diffraction pattern of an as-synthesized sample. A further increase of the temperature above 300 °C reveals a decomposition of POROF-2, as confirmed by combined powder X-ray diffraction and FT-IR characterization. Such a thermal stability is remarkable since most nanoporous organic materials reported to date incorporate guest solvent molecules, that once eliminated, induce a collapse of the crystalline material. To our knowledge, there are only a few previous examples of nanoporous organic hydrogen-bonded networks that remain ordered even when most of the guest molecules are removed.[17]

Variable-temperature magnetic-susceptibility data for a crystalline sample of POROF-2 was obtained on a SQUID susceptometer, under a temperature range of 2–300 K and an applied magnetic field of 200 Oe (see inset Figure 3). The χT

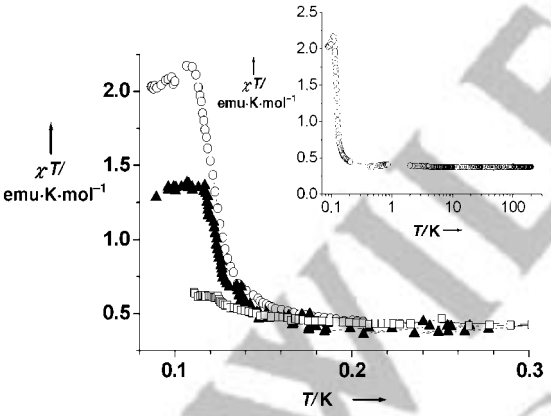

Figure 3: χT as a function of temperature for different applied magnetic fields H: (○) $H = 200$ Oe, (▲) $H = 500$ Oe, and (□) $H = 1000$ Oe. The inset shows the logarithmic dependence of χT function on the temperature up to 200 K, measured with an applied magnetic field of 200 Oe.

value at 300 K is 0.38 emu K mol^{-1}, which is in agreement with the theoretical value expected for a noninteracting $S = 1/2$ spin in each molecule. Upon cooling, the χT value remains constant down to 5 K, whereupon the χT value increases according with the presence of weak ferromagnetic interactions. This behavior was fitted to the Curie–Weiss law with a Weiss constant of $\theta = +0.2$ K. To investigate the existence of magnetic ordering at very low temperatures, variable temperature magnetic susceptibility experiments down to 0.07 K were performed in a dilution cryostat (see Figure 3). A considerable increase of the χT value up to a maximum around 0.110 K was observed on cooling down below 2 K,

which shows a transition to a ferromagnetic ordered state at very low temperatures. The intensity of the peak decreases whereas its maximum shifts slightly to higher temperatures on increasing the external applied magnetic field. For instance, for an applied magnetic field of 20 Oe ■■ok? 200 Oe in Figure 3■■ a value of 2.2 emu K mol^{-1} was obtained, whereas for an external field of 50 Oe ■■ok? 500 Oe in Figure 3■■ the value is reduced to 1.4 emu K mol^{-1}. This behavior originates in the saturation of magnetization for fields of few hundred Oe. Magnetization curves were measured above and below the critical temperature and are illustrated in Figure 4. At 1.35 K, POROF-2 remains in the paramagnetic region and therefore the magnetization curve has a slight gradient. On the contrary, the curve at 0.80 K, even if it is very close to the critical temperature, traces a hysteretic loop characteristic of a soft ferromagnet. The magnetization is almost saturated at about 400 Oe, and though the coercitive force is of the order of 50 Oe (see inset of Figure 4), the remnant magnetization at zero field is

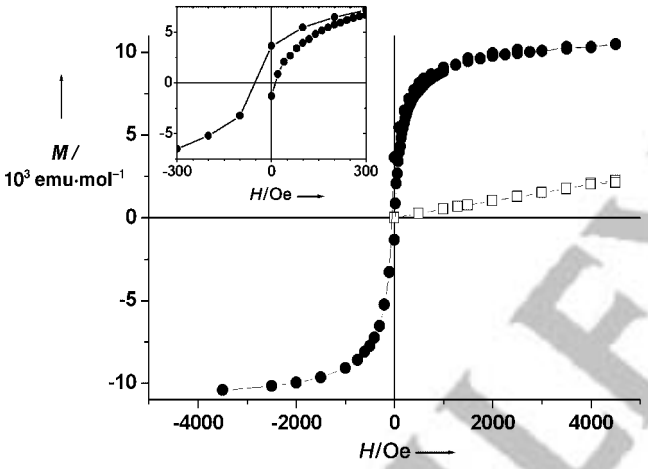

Figure 4: Magnetization curves as a function of the applied magnetic field, measured at different temperatures. (●) 0.08 K, (□) 1.35 K. The inset shows the detail of the curve at 0.08 K around zero field.

of about 35% of the saturation value.

In conclusion, we have reported the first example of a supramolecular, nanoporous purely organic, "zeolite-like" material exhibiting an unusual thermal stability, a hydrophilic nanoporous architecture, and a long-range ferromagnetic ordering. Nanoporous materials exhibit a wide range of applications, such as molecular sieves, catalysis, separation, and sensors. Such properties, along with the magnetic properties of the organic framework, may open a new avenue to the development of new multifunctional materials.

Experimental Section

Radical **2**: A mixture of tris(2,3,4,5-tetraclorophenyl)methane[18] (1.70 g, 2.58 mmol), chloroform (30 mL), and aluminum chloride (0.40 g, 3.00 mmol) was heated at 160 °C for 8 h in a glass pressure vessel. The mixture was then poured onto ice/1N hydrochloric acid and extracted with chloroform. The white solid collected was mixed in 20% oleum (100 mL) and heated at 150 °C for 12 h. The final solution

was cooled and poured into cracked ice. The solid was washed with water, dissolved in Et_2O, extracted with aqueous sodium hydrogen carbonate, acidified, extracted with Et_2O, and dried in vacuo. A solution of the resultant white precipitate in DMSO was shaken with an excess of powdered NaOH for 72 h. The mixture was filtered and immediately a stoichiometric amount of iodine was added to the filtrate■■ok?■■. The solution was left undisturbed in the dark (45 min), washed with an aqueous solution of sodium hydrogen sulfite (■■ M, ■■ mL), and treated with Et_2O (■■ mL). Radical **2** was extracted with aqueous sodium hydrogen carbonate, and this aqueous layer was acidified and extracted with Et_2O. The extracted solid was recrystallized from Et_2O/*n*-pentane to give radical **2** as red powder. IR (KBr): $\tilde{\nu}$ = 3500–2500, 1740, 1694, 1662, 1537, 1441, 1408, 1352, 1326, 1290, 1251, 1226, 1040, 931, 752, 722, 665, 574, 522, 462 cm^{-1}. Elemental analysis (%) calcd: C 33.50, H 0.38; found C 33.65, H 0.32. Crystals suitable for X-ray diffraction were grown from a mixture of dichloromethane and *n*-hexane.

Received: November 19, 2003 [Z53358]

Keywords: ferromagnetism · magnetic properties · nanoporous materials · radicals · zeolite analogues

[1] a) *Magnetic Properties of Organic Materials* (Ed.: P. M. Lahti), Marcel Dekker, New York, **1999**, and references therein; b) J. Veciana, H. Iwamura, *MRS Bull.* **2000**, *25*, 41, and references therein.

[2] M. Tamura, Y. Nakazama, D. Shiomi, K. Nozawa, Y. Hosokoschi, M. Ishikawa, M. Takahashi, M. Kinoshita, *Chem. Phys. Lett.* **1991**, *186*, 401.

[3] a) A. Alberola, R. L. Less, C. M. Pask, J. M. Rawson, F. Palacio, P. Oliete, C. Paulsen, A. Yamaguchi, R. D. Farley, D. M. Murphy, *Angew. Chem.* **2003**, *115*, 4930; *Angew. Chem. Int. Ed.* **2003**, *42*, 4782; b) M. M. Matshushita, A. Izuoka, T. Sugawara, T. Kobayashi, N. Wada, N. Takeda, Ishikawa, *J. Am. Chem. Soc.* **1997**, *119*, 4369; c) A. J. Banister, N. Bricklebank, I. Lavender, J. M. Rawson, C. I. Gregory, B. K. Tanner, W. Clegg, M. R. J. Elsegood, F. Palacio, *Angew. Chem.* **1996**, *108*, 2648; *Angew. Chem. Int. Ed. Engl.* **1996**, *35*, 2533; d) J. Cirujeda, M. Mas, E. Molins, F. Lanfranc de Panthou, J. Laugier, Je. G. Park, C. Paulsen, P. Rey, C. Rovira, J. Veciana, *J. Chem. Soc. Chem. Commun.* **1995**, 709; e) A. Caneschi, F. Ferraro, D. Gatteschi, A. le Lirzin, E. Rentschler, R. Sessoli, *Adv. Mater.* **1995**, *7*, 476; f) M. P. Allemand, K. C. Khemani, A. Koch, F. Wudl, K. Holczer, S. Donovan, G. Grüner, J. D. Thompson, *Science* **1991**, *253*, 301; g) R. Chiarelli, M. A. Novak, A. Rassat, J. L. Tholance, *Nature* **1993**, *363*, 147; h) K. Awaga, T. Inabe, Y. Maruyama, *Chem. Phys. Lett.* **1992**, *190*, 349; i) T. Sugano, M. Tamura, M. Kinoshita, Y. Sakai, Y. Ohashi, *Chem. Phys. Lett.* **1992**, *200*, 235.

[4] a) J.-M. Lehn, *Supramolecular Chemistry*, VCH, Weiheim, **1995**; b) C. B. Aakeröy, A. M. Beatty, B. A. Helfrich, *Angew. Chem.* **2001**, *113*, 3340; *Angew. Chem. Int. Ed.* **2001**, *40*, 3240.

[5] a) T. Otsuka, T. Okuno, K. Awaga, T. Inabe, *J. Mater. Chem.* **1998**, *8*, 1157; b) T. Akita, Y. Mazakati, K. Kobayashi, *J. Chem. Soc. Chem. Commun.* **1995**, 1861; c) J. Cirujeda, L. E. Ochando, J. M. Amigo, C. Rovira, J. Ruis, J. Veciana, *Angew. Chem.* **1995**, *107*, 99; *Angew. Chem. Int. Ed. Engl.* **1995**, *34*, 55; d) J. Cirujeda, E. Hernandez-Gasio, C. Rovira, J. L. Stanger, P. Turek, J. Veciana, *J. Mater. Chem.* **1995**, *5*, 243; e) F. M. Romero, R. Ziessel, M. Bonnet, Y. Pontillon, E. Ressouche, J. Schweitzer, B. Delley, A. Grand, C. Paulsen, *J. Am. Chem. Soc.* **2000**, *122*, 1298.

[6] a) J. Veciana, J. Cirujeda, C. Rovira, J. Vidal-Gancedo, *Adv. Mater.* **1995**, *7*, 221; b) E. Hernandez, M. Mas, E. Molins, C. Rovira, J. Veciana, *Angew. Chem.* **1993**, *105*, 919; *Angew. Chem. Int. Ed. Engl.* **1993**, *32*, 882.

[7] M. Ballester, *Acc. Chem. Res.* **1985**, *18*, 380.
[8] D Maspoch, P. Gerbier, L. Catala, J. Vidal-Gancedo, K. Wurst, C. Rovira, J. Veciana, *Chem. Eur. J.* **2002**, *8*, 3635.
[9] S. V. Kolotuchin, P. A. Thiessen, E. E. Fenlon, S. R. Wilson, C. J. Loweth, S. C. Zimmerman, *Chem. Eur. J.* **1999**, *5*, 2537, and references therein.
[10] For a general review, a) A. Nangia, *Curr. Opin. Solid State Mater. Sci.* **2001**, *5*, 115; b) M. J. Zaworotko, *Angew. Chem.* **2000**, *112*, 3180; *Angew. Chem. Int. Ed.* **2000**, *39*, 3052; c) P. J. Langley, J. Hulliger, *Chem. Soc. Rev.* **1999**, *28*, 279; d) G. R. Desiraju, *Curr. Opin. Solid State Mater. Sci.* **1997**, *2*, 451.
[11] a) Y. Miyahara, K. Abe, T. Inazu, *Angew. Chem.* **2002**, *114*, 3146; *Angew. Chem. Int. Ed.* **2002**, *41*, 3020; b) D. T. Bong, M. R. Ghadiri, *Angew. Chem.* **2001**, *113*, 2221; *Angew. Chem. Int. Ed.* **2001**, *40*, 2163; c) K. Sada, M. Sugahara, K. Kato, M. Miyata, *J. Am. Chem. Soc.* **2001**, *123*, 4386; d) Y. H. Kiang, S. Lee, Z. Xu, W. Choe, G. B. Gardner, *Adv. Mater.* **2000**, *12*, 767; e) T. Müller, J. Hulliger, W. Seichter, E. Weber, T. Weber, M. Wübbenhorst, *Chem. Eur. J.* **2000**, *6*, 54; f) K. Kobayashi, T. Shirasaka, A. Sato, E. Horst, N. Furukawa, *Angew. Chem.* **1999**, *111*, 3692; *Angew. Chem. Int. Ed.* **1999**, *38*, 3483; g) K. Biradha, D. Dennis, V. A. MacKinnon, C. V. K. Sharma, M. J. Zaworotko, *J. Am. Chem. Soc.* **1998**, *120*, 11894; h) V. C. Russel, C. C. Evans, W. Li, M. D. Ward, *Science* **1997**, *276*, 575.
[12] D. Maspoch, N. Domingo, D. Ruiz-Molina, K. Wurst, J. Tejada, C. Rovira, J. Veciana, *J. Am. Chem. Soc.*, submitted.
[13] X-ray single-crystal diffraction data for POROF-2 was collected on a Kuma KM-8 diffractometer with a CCD area detector and silicon-monochromized synchroton radiation ($\lambda = 0.53378$ Å) Crystal data for OROF-2: trigonal, space group $P\bar{3}c1$, dimensions $0.15 \times 0.15 \times 0.01$ mm, $a = 15.9283(7)$, $b = 15.9283(7)$, $c = 13.8886(11)$ Å, $V = 3051.6(3)$ Å^3, $Z = 4$, $\lambda = 0.53378$ Å, $\mu = 0.572$ mm^{-1}. A total range of 24868 reflections were collected in the range of $1.0 \leq \theta \leq 20.5$, of which 2232 were unique reflections. Least-squares refinement based on 2084 reflections with $I > 2\sigma(I)$ led to converge, with a final $R1 = 0.0585$, $wR2 = 0.1418$, and GOF = 1.133. CCDC-223669 (POROF-2) contains the supplementary crystallographic data for this paper. These data can be obtained free of charge via www.ccdc.cam.ac.uk/conts/retrieving.html (or from the Cambridge Crystallographic Data Centre, 12 Union Road, Cambridge CB2 1EZ, UK; fax: (+44) 1223-336-033; or deposit@ccdc.cam.ac.uk).
[14] a) A. Noman, M. M. Rahman, R. Bishop, D. C. Craig, M. L. Scudder, *Chem. Commun.* **1999**, 2389; b) R. K. R. Jetti, P. K. Thallapally, F. Xue, T. C. W. Mak, A. Nangia, *Tetrahedron* **2000**, *56*, 6707; c) R. K. R. Jetti, F. Xue, T. C. W. Mak, A. Nangia, *Cryst. Eng.* **1999**, *2*, 215.
[15] Determined using A. M. C. T. PLATON, Utrecht University, Utrecht, The Netherlands, Spek, A.L. **1998** ■■ok?■■.
[16] Indeed, even though Kitaigorodski's principle of close crystal packing originates from the idea that organic building blocks tend to interpenetrate, several purely organic nanoporous structures have already been obtained. See refs. [9] and [10].
[17] a) P. Sozzani, A. Comotti, R. Simonutti, T. Meersman, J. W. Logan, *Angew. Chem.* **2000**, *112*, 2807; *Angew. Chem. Int. Ed.* **2000**, *39*, 2695; b) P. Brunet, M. Simard, J. D. Wuest, *J. Am. Chem. Soc.* **1997**, *119*, 2737; c) A. T. Ung, D. Gizachew, R. Bishop, M. L. Scudder, I. G. Dance, D. C. Craig, *J. Am. Chem. Soc.* **1995**, *117*, 8745; d) B. T. Ibragimov, S. A. Talipov, *J. Inclusion Phenom. Mol. Recognit. Chem.* **1994**, *17*, 317.
[18] M. Ballester, J. Riera, J. Castañer, C. Rovira, O. Armet, *Synthesis* **1986**, 64.

Supporting Information

A New Robust Pure Organic Nanoporous Magnet.

Daniel Maspoch, Neus Domingo, Daniel Ruiz-Molina, Klaus Wurst, Gavin Vaughan, Javier Tejada, Concepció Rovira and Jaume Veciana*

---

[*] Prof. J. Veciana, Dr. Concepció Rovira, Dr. D. Ruiz-Molina, D. Maspoch
Institut de Ciencia de Materials de Barcelona (CSIC), Campus Universitari de Bellaterra 08193, Cerdanyola, Spain
Prof. J. Tejada, N. Domingo.
Facultad de Física, Universitat de Barcelona, Diagonal 647, 08028-Barcelona, Spain.
Dr. K. Wurst
Institut für Allgemeine, Anorganische und Theoretische Chemie, Universität Innsbruck, Innrain 52a, A-6020, Innsbruck, Austria
Dr. Gavin Vaughan
European Syncrotron Radiation Facility (E.S.R.F.), B. P. 220, F - 38043 Grenoble cedex, France.

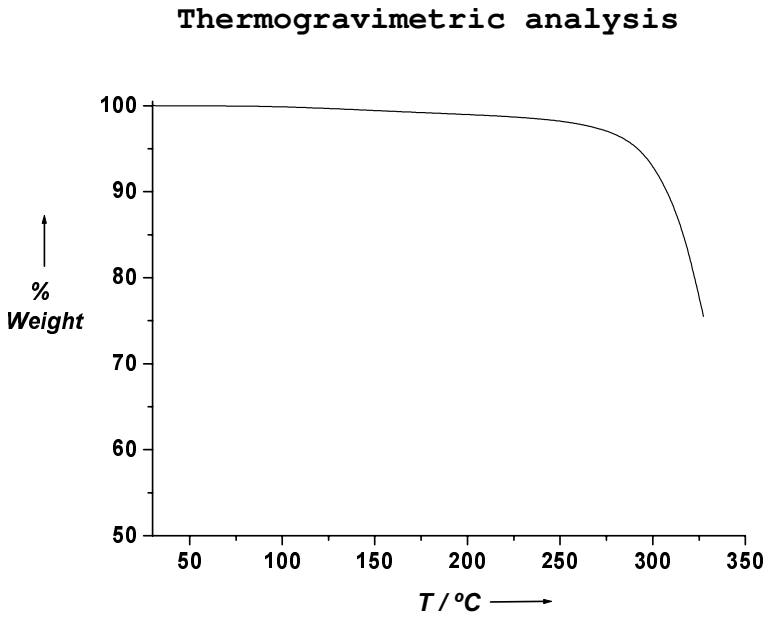

Fig 1. Thermal gravimetric study of a few single crystals of as-synthesized POROF-2

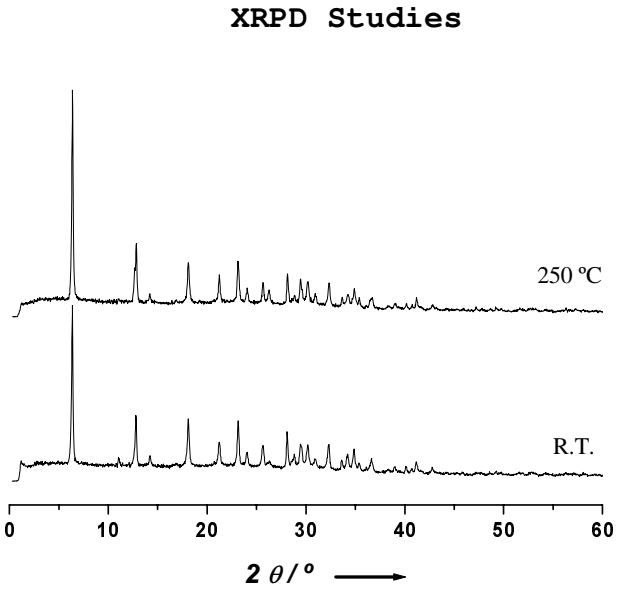

Fig 2. X-ray powder diffractogram of POROF-2 at R.T. and 250ºC